Solar Physics (2006) 239: 337–392
DOI: 10.1007/s11207-006-0132-3

PROPERTIES OF STREAM INTERACTIONS AT ONE AU DURING 1995 – 2004

L. JIAN
Institute of Geophysics and Planetary Physics, University of California, Los Angeles,
595 Charles E. Young Dr. East, 6862 Slichter, Los Angeles, CA 90095, U.S.A.
(e-mail: jlan@igpp.ucla.edu)

C.T. RUSSELL
Institute of Geophysics and Planetary Physics, University of California, Los Angeles,
595 Charles E. Young Dr. East, 6869 Slichter, Los Angeles, CA 90095, U.S.A.
(e-mail: ctrussel@igpp.ucla.edu)

J.G. LUHMANN
Space Sciences Laboratory, University of California, Berkeley, CA 94720, U.S.A.
(e-mail: jgluhman@ssl.berkeley.edu)

and

R.M. SKOUG
Los Alamos National Laboratory, Los Alamos, NM 87545, U.S.A.
(e-mail: rskoug@lanl.gov)

(Received 10 January 2006; accepted 23 October 2006; Published online 6 December 2006)

Abstract. A stream interaction region (SIR) forms when a fast solar stream overtakes a slow stream, leading to structure that evolves as an SIR moves away from the Sun. Based on *Wind* (1995 – 2004) and ACE (1998 – 2004) *in situ* observations, we have conducted a comprehensive survey of SIRs at one AU, including a separate assessment of the longer-lasting corotating interaction regions (CIRs) that recur on more than one solar rotation. In all there are 196 CIRs, accounting for about 54% of the 365 SIRs. The largest proportion of CIRs to SIRs (64%) appears in 1999, and the smallest proportion (49%) is in 2002. Over the ten years, the annual number of SIR events varies little, from 32 up to 45. On average, the occurrence rate of shocks at SIRs at one AU is about 24%. Seventy percent of the SIRs with shocks have only forward shocks, more than twice the percentage of SIRs with only reverse shocks. This preponderance of forward shocks is consistent with the deflections of forward and reverse shocks relative to the ecliptic plane. In order to help address the effect of SIRs and CIRs on geomagnetic activity, we determine the solar-cycle variation of the event duration, scale size, the change in velocity from slow stream to fast stream, and the solar-cycle variation of the maximum magnetic field, peak total perpendicular pressure, and other properties. These statistics also provide a baseline for future studies at other heliocentric distances and for validating heliospheric models.

1. Introduction

The coronal magnetic structure modulates the solar wind structure (*e.g.*, Pneuman and Kopp, 1971). For much of the solar cycle, the magnetic field in the corona, well above the photosphere, is roughly that of a dipole, tilted with respect to the rotation axis of the Sun (*e.g.*, Gosling and Pizzo, 1999). As the solar magnetic field evolves in the course of the Sun's 11-year solar activity cycle, this tilt varies, producing a change in the configuration of the heliospheric current sheet. The dipole tends to be nearly aligned with the rotation axis near solar-activity minimum (*e.g.*, Hundhausen, 1977), whereas it tends to be inclined substantially relative to the solar-rotation axis in the declining phase of the solar cycle. Near the activity maximum, the solar magnetic field is complex, but recent *Ulysses* work concluded that the dipole approximation is reasonable throughout the solar cycle (*e.g.*, Jones, Balogh, and Smith, 2003).

Fast and tenuous streams originate in coronal holes (Krieger, Timothy, and Roelof, 1973), while the relatively slow and dense streams arise in the streamer belt (Feldman *et al.*, 1981; Gosling *et al.*, 1981). They are quite distinct in their kinetic properties. Because the slow stream and fast stream are radially aligned and originate from different positions on the Sun at different times, their frozen-in magnetic fields are different, preventing the two streams from interpenetrating (Gosling and Pizzo, 1999). Therefore, when they move away from the Sun, the fast stream collides with the slow stream ahead, while simultaneously outrunning the slow trailing stream. This forms a compression on the rising-speed portion of the slow stream and a rarefaction on the trailing edge of the fast stream, as indicated in Figure 1 (*e.g.*, Parker, 1963; Sarabhai, 1963; Carovillano and Siscoe, 1969; Gosling *et al.*, 1972; Hundhausen, 1972; Siscoe, 1972), denoted as the acceleration phase and deceleration phase respectively in Section 5.

If the flow pattern emanating from the Sun is roughly time-stationary, then the stream interaction regions form spirals in the solar equatorial plane that corotate with the Sun and are commonly called corotating interaction regions (CIRs) (Smith and Wolfe, 1976; Gosling and Pizzo, 1999). Because of the temporal variability in the solar-wind structures, a fast stream coming from a given point may vanish before the Sun rotates completely and not produce a periodic stream interaction. Even stream interactions with poor recurrence, though, may still be strong while they exist and affect geomagnetic activity (*e.g.*, Bobrov, 1983). Following the suggestion of Gosling *et al.* (2001), in this study we use the term "stream interaction regions" (SIRs), to include such transient and possibly localized stream interactions. In the following sections, we provide a comprehensive examination of the statistics of the SIRs properties (with CIRs specified separately) at one AU over the period 1995 –2004.

The boundary separating the originally fast, tenuous, and hot wind of the fast stream from the slow, dense, and cold stream, was first studied by Belcher and Davis (1971). In 1974, Burlaga named this boundary the "stream interface" (SI), and subsequently it was examined in detail by Gosling *et al.* (1978). They found that the SI is distinguished as an abrupt drop in particle density accompanied by a simultaneous rise in proton temperature. Intriligator and Siscoe (1994) noted that this signature was that of a relatively abrupt increase in specific entropy. More recently, Wimmer-Schweingruber, von Steiger, and Paerli (1997, 1999) used the data from the solar-wind ion-composition spectrometer (SWICS)/*Ulysses* instrument, to show additional evidence that the stream interface separates plasmas originating in

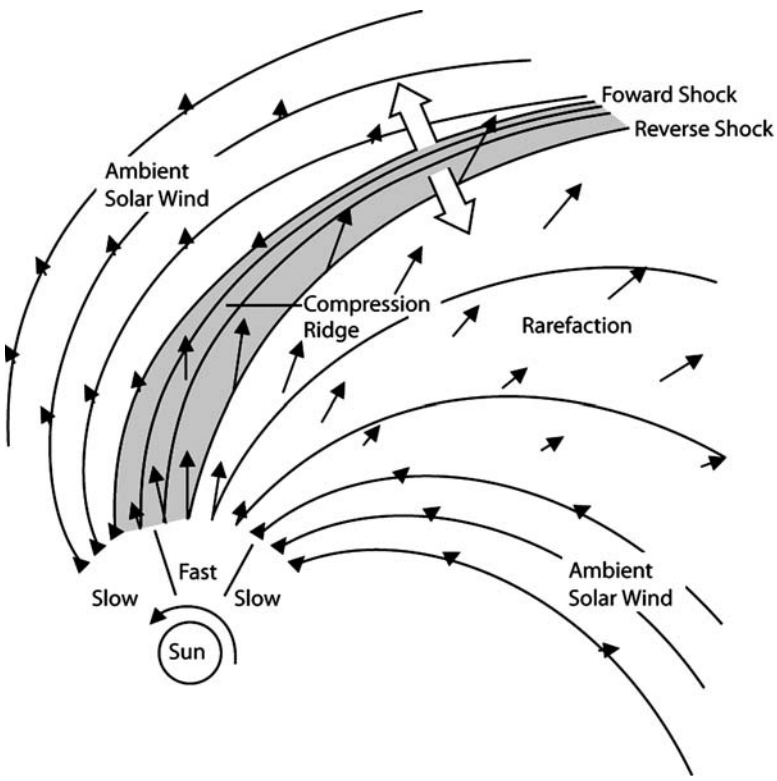

Figure 1. Schematic illustrating 2-D corotating stream structure in the solar equatorial plane in the inner heliosphere (after Pizzo, 1978).

different coronal and chromospheric regions. Later, Gosling and Pizzo (1999) pointed out that the plasma pressure within a CIR peaks in the vicinity of the stream interface, where there is a large shear in the flow.

The interaction between fast and slow streams starts in the inner heliosphere (*e.g.*, Richter and Luttrell, 1986), and the interaction region broadens with increasing heliocentric distance. Far out in the heliosphere, the SIRs eventually coalesce.

2. Total Perpendicular Pressure

Magnetic field and plasma both contribute to the pressure, but the magnetic field cannot exert a gradient pressure force parallel to the field. The total perpendicular pressure (P_t) is the sum of the magnetic pressure and plasma thermal pressure perpendicular to the magnetic field [$B^2/(2\mu_0) + \sum_j n_j k T_{\mathrm{perp},j}$, where j represents proton, electron, and α particle] (estimated as total pressure in Gosling *et al.*, 1987, 1994; Gosling, 1990). Since it is the gradient of the combined pressure that drives the evolution of solar-wind structures, much simpler signatures arise in P_t than in the signatures of the constituent components.

This simple pressure pattern that we exploit herein has been demonstrated in earlier work, *e.g.*, Gosling (1990), Gosling and Pizzo (1999). The pressure reaches a maximum at the stream interface. The peak pressure is equal to the dynamic pressure of the flow on either side of the SI resolved along the normal to the boundary and in the boundary reference frame. Since the variations of the individual plasma properties may not occur simultaneously, the maximum pressure point provides a robust and quick means to identify the SI passage time (Jian *et al.*, 2005a).

Generally, irregularities in P_t are smoothed by compressional waves that radiate away pressure inhomogeneities. However, when the velocity change across the plasma interface exceeds the compressional wave speed, shocks arise and produce discontinuities in pressure (converted from the dynamic pressure of the flow in the discontinuity frame) because they are supersonic, and cannot mitigate the steep gradient with small amplitude waves.

3. Criteria of Stream Interaction Regions

A stream interaction region can occur only if a fast stream overtakes a slower stream, ensuring that the solar-wind velocity increases across the stream interface. A P_t gradient arises to deflect the plasma flow that, in the SI frame, flows toward the interface from both sides. In other words, the dynamic pressure of the flow on both sides of the interface expressed in the interface frame is balanced by P_t centered on the interface.

So, our criteria for SI identification are first that the solar-wind speed must be increasing and second that P_t reaches a maximum. Other characteristics such as the compression of proton number density and magnetic field at the interface are also required, and the flow deflection and temperature increase at the interface give additional assurance of a correct identification.

In order to distinguish SIRs from interplanetary coronal mass ejections (ICMEs), we describe some features of ICMEs briefly. For more details, please refer to our parallel study of ICME properties at one AU during 1995 – 2004 (Jian *et al.*, 2006). First, ICMEs are characterized by a high-density sheath of compressed solar wind, followed by a normal to low-density and low-β region, with low variance, and often a large magnitude and rotating magnetic field that lasts one day or two. Second, in contrast to the SIR's peak with a slow increase and decrease of pressure on its two sides, ICMEs usually can be characterized as having three types of P_t behavior (Jian *et al.*, 2005b, 2006; Russell, Shinde, and Jian, 2005): a broad pressure maximum near the event center, a sharp rise followed by a steady plateau and then a return to pre-event pressures, and a rise followed by a gradual, possibly exponential, decay, respectively. We think they may represent the impact parameter of the spacecraft relative to the central flux rope.

A minority of ICMEs and SIRs have irregular P_t profiles, usually caused by interactions of more than one event. Nevertheless, since our identification is done by eye, rather than by a numerical algorithm, the specific and thorough examination of the velocity, proton temperature, magnetic field and other features as well as the background solar wind content, makes us confident in our identification.

In addition, the variations of SIRs appearance may be partially caused by transient components of the slow solar wind associated with either slow coronal-mass ejections (CMEs) at the Sun, plasmoids formed at the edges of the coronal streamer belt, or by transients associated with the temporally evolving boundaries of the open-field source regions of the solar wind. All of these transient structures presumably become part of the slow-wind belt, and can affect it differently at different times and locations. In this study, we do not attempt to determine whether an SIR is affected by one or more of these structures because there is no straightforward way to unambiguously identify their contributions. However, it is important to appreciate that such differences exist in some SIRs, and may affect their P_t behavior and other features.

4. List of Stream Interaction Regions

From the *Ulysses* observations at southern latitudes during its first orbit (1992), the onset of the recurrent high-speed stream occurred at a solar latitude of -13° and marked the exit from the streamer-belt-dominated region at around five AU (Bame *et al.*, 1993). Nevertheless, the solar wind is often more complex than was observed during the first *Ulysses* orbit (*e.g.*, McComas *et al.*, 2006). In this study, we use *Wind* (1995 – 2004) and *Advanced Composition Explorer* (ACE) (1998 – 2004), which are both close to the equatorial plane at about one AU.

Proton data are nearly always available. However, the electron temperature (T_e), α temperature, the ratio of α number density to proton density, and the anisotropy of these particles' temperature, are less often available. Consistent with the high thermal conductivity of electrons and the low correlation of T_e with other solar-wind parameters (*e.g.*, Newbury *et al.*, 1998, and references therein), we assume a constant and isotropic T_e. Because the average value of electron core temperature varies from $\sim$123 000 K in 1996 around up to $\sim$144 000 K in 2001 near solar maximum (Issautier *et al.*, 2005), herein we set the electron perpendicular temperature as 130 000 K for all ten years. This value is close to the median electron temperature in Newbury *et al.* (1998) from 18 months' continuous observation of the *International Sun-Earth Explorer* (ISEE)-3. Considering the relatively minor effects of α particles and the ion-temperature anisotropy on the P_t, we also assume a constant 4% composition (by number) of α particles with a temperature four times that of the protons, and the isotropy of ion temperature. The discrepancy between these assumptions and the real values will slightly affect the P_t profiles; nevertheless it should make little change in our statistics.

Under these assumptions, we have calculated P_t for the entire *Wind* [SWE (Ogilvie *et al.*, 1995) and MFI (Lepping *et al.*, 1995), both in 93-second time resolution] solar-wind data set and ACE [validated Level 2 of SWEPAM (McComas *et al.*, 1998) and MAG (Smith *et al.*, 1998), both in 64-second time resolution] solar-wind data set. Because *Wind* has been gathering data longer, we started our list of events by examining the *Wind* data. When *Wind* is in the magnetospherically susceptible region, or has data gaps or noisy data, we use ACE data to provide a more complete survey of SIR events. Using a time window of one solar-rotation cycle, *i.e.* 25 – 29 days, we determine the recurrence of stream interactions. If an SIR recurs on two or more solar rotations, it is also a CIR in this study. All SIR events are listed in the Appendix*, with those SIRs that are also CIRs indicated in the CIR column.

Since the *Wind* trajectory changes from an L_1 orbit into a series of Earth orbits, while ACE stays near the L_1 point, the combination of the two spacecraft introduces a difference in the timing of the signature of the order of one hour. Because the SIRs are large in spatial scale (also demonstrated by the mean size of SIRs from our survey in Section 7), the observations of the two spacecraft are otherwise similar, as long as *Wind* is not too close to the Earth where its measurement can be affected by the Earth's magnetosphere. In addition, we do not consider evolution over the rather short separation between the two spacecraft, nor would we expect any significant evolution. Thus, we do not make the lists from *Wind* or ACE separately, but rather identify the data source as "ACE" in comments if it is from ACE data.

During 1995 – 1997, only *Wind* observations are available. There are gaps in the solar-wind data for periods of only about 3.8%, 7.6%, and 3.7% in each of these years, respectively. Since these outages are smaller than the expected statistical variability, we feel we do not need to make significant corrections to our following statistics.

Through the study, we define the boundary from a consensus of the available signatures described in Section 3, with an emphasis on the central maximum above the ambient solar wind in the composed P_t profile, *i.e.* the interval covers where the pressure structure emerges from and decays back to the background. Often, the rapid jump in P_t and other parameters is a good separator of the SIR from the background.

We record ΔP as the instantaneous change of P_t across a discontinuity, P_{max} and B_{max} as the peaks of P_t and $|\mathbf{B}|$, R_V as the ratio of V_{max} to V_{min}, ΔV as the change in the solar-wind speed magnitude, which is important to the evolution of the stream interaction, D_{before} as the duration between the start time and the stream interface (SI), D_{after} as the duration between the SI and the end time, R_d as the ratio of D_{before} to D_{after} to imply the temporal asymmetry relative to SI for each event. Lastly, we estimate the SIR scale size based on the measured duration and the average velocity, the latter being the mean of V_{max} and V_{min}. Because the P_t in the background solar wind is typically only 20 – 30 pPa, and the relative interaction strength between events is of primary interest, we can just consider the P_{max} magnitude rather than the difference between it and the background P_t.

*__Electronic Supplementary Material__ Supplementary material is available for this article at http://dx.doi.org/10.1007/s11207-006-0132-3

In addition, we note some SIRs have an irregular P_t profile, with several small spikes, or are relatively flat, like a plateau. For these events, we determine the SI crossing from the consensus of P_t peak and also the characteristic variations in other parameters, such as N_P, T_P, and so on. As commented in the Appendix, some SIRs do not have sharp interfaces between slow and fast streams, but gradual transitions, where N_P, T_P, and other parameters change gradually.

For a discontinuity simply indicated by P_t, we examine V_P, N_P, T_P, and **B** one by one, and when necessary, also use the high-time-resolution *Wind* 3DP (Lin *et al.*, 1995) and MFI, ACE SWEPAM, and magnetometer data from CDAWeb, to determine whether it is a forward or reverse shock. As is well known, at forward shocks, the solar-wind speed increases, while simultaneously N_P and T_P both are enhanced; at reverse shocks, solar-wind speed again increases, while N_P and T_P both decline. We have double-checked our shock identification with the shock lists from Kasper (*http://space.mit.edu/home/jck/shockdb/shockdb.html*), the ACE team (*http://www-sg.sr.unh.edu/mag/ace/ACElists/obs_list.html*), *etc*.

5. Examples of SIR Events

Figures 2 and 3 display two interesting SIR examples. They are in the same format. The first three panels (B_x/B, B_y/B, B_z/B), are the direction cosines of the interplanetary magnetic field (IMF) in geocentric solar magnetospheric (GSM) coordinates. In the following panels: $|\mathbf{B}|$ is the magnetic-field strength; V_P is the solar-wind speed magnitude; N_P is the proton number density; T_P is the proton temperature; β is the ratio of plasma thermal pressure to the magnetic pressure, and P_t is the total perpendicular pressure, in the unit of pico-Pascal (pPa).

We do not use cone angle, $\arccos(B_x/B)$, and clock angle, $\arctan(B_y/B_z)$ of IMF, because the use of these angles assumes a particular symmetry around the direction to the Sun which is not present in SIRs. We conduct the statistical study using scalar parameters, independent of coordinates (*e.g.*, GSE *vs.* GSM). However, any future geoeffectiveness study requires GSM coordinates. Thus, we use GSM coordinates.

Figure 2 illustrates an SIR without shocks, indicated by the dashed lines *a* and *c*. The P_t profile is simple: an increase and then a decrease of P_t both occurring during an increasing speed profile, individually corresponding to an acceleration phase of slow stream, and a deceleration phase of fast stream. The components vary in a complex way. Within about half a day before the stream interface, B_x/B, B_y/B, B_z/B shift their polarities distinctly, possibly due to a nearby sector boundary. There is a varying magnetic field strength, a constant temperature, and a density rise in the acceleration phase; and a sharp density drop around the SI, marked by the dashed line *b*; then the density and temperature both gradually decline in the deceleration phase. The SI separating the fast and slow streams, is relatively thin and not resolved by these data.

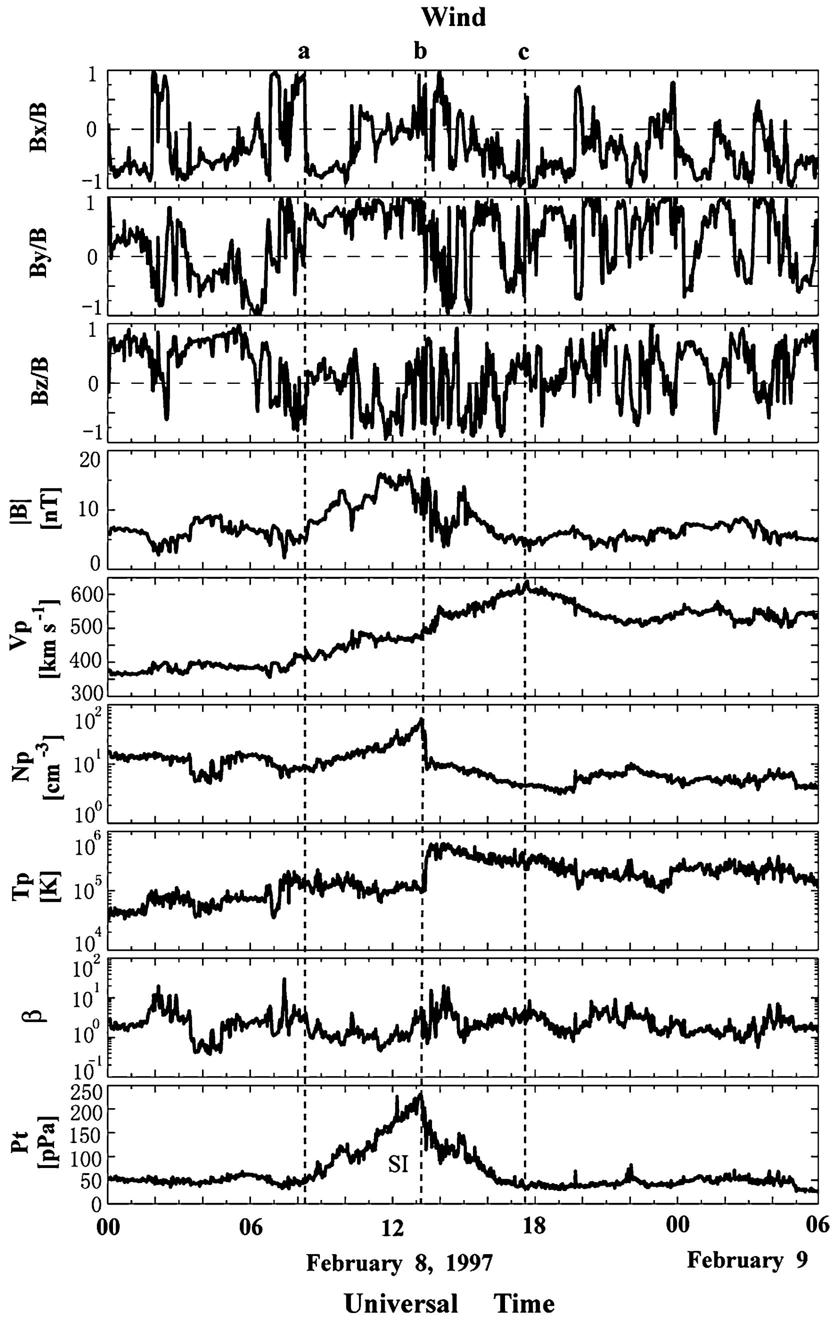

Figure 2. SIR event without shocks, from *Wind* data. From top to bottom: direction cosines of IMF in GSM coordinates, magnetic-field strength, solar-wind speed, proton density, proton temperature, β, and total perpendicular pressure. Dashed lines *a* and *c* indicate the boundaries of the SIR; dashed line *b* marks the stream interface (SI).

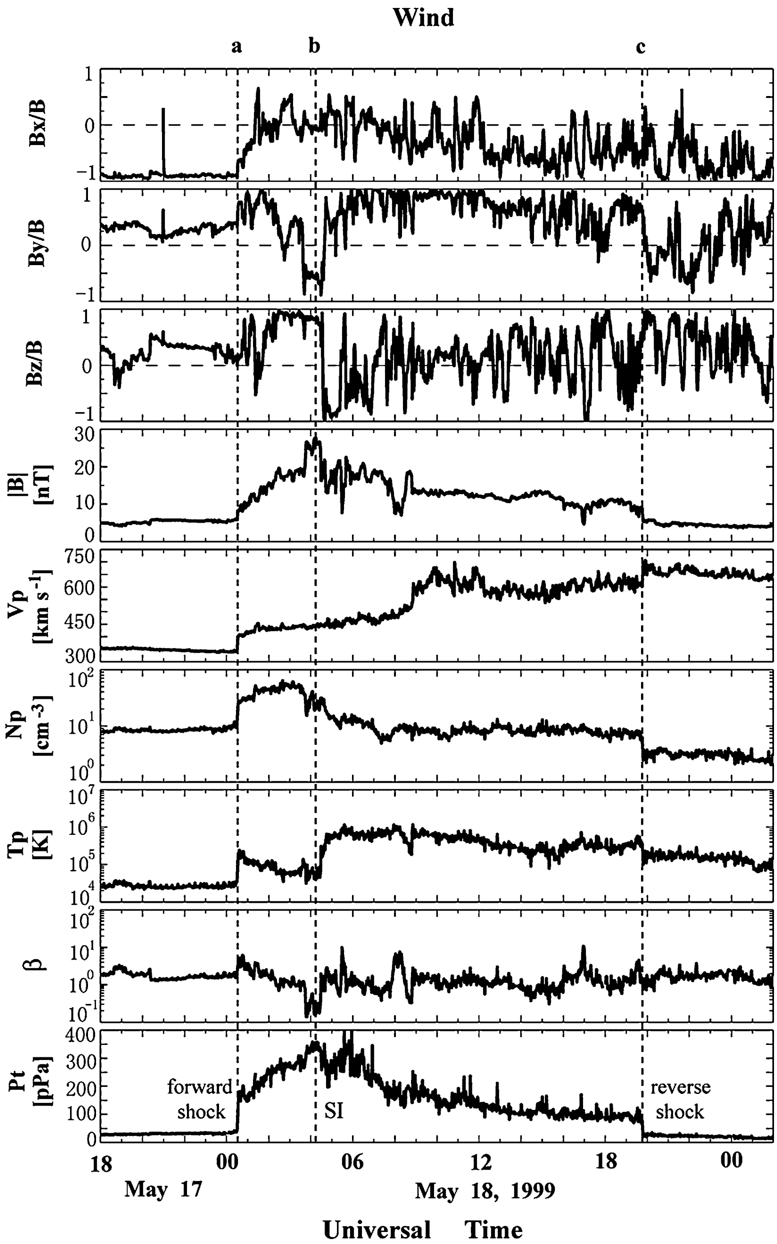

Figure 3. SIR event with a pair of forward – reverse shocks, following the same format as described for Figure 2. Dashed lines *a* and *c* mark the pair of forward and reverse shocks bounding the SIR; dashed line *b* indicates the stream interface (SI).

On the low-speed (left-hand) side of the interface, there is no correlation of the magnetic-field strength, density, and temperature as one might expect in the compression region, so clearly marked by the pressure rise, had it been formed in uniform plasma. Clearly on the slow-stream side, a structured source region dominates compression in creating the observed structure at the interface. On the high-speed side, there is a better, but not complete, correlation between the field strength, the density, and the temperature, suggesting greater uniformity in the source region of this flow.

Figure 3 shows an SIR with a P_t enhancement bounded by a pair of forward-reverse shocks (dashed lines *a* and *c*). Here the component variations are more complex. The acceleration phase of the slow stream has a temperature decrease while P_t increases. The deceleration phase of the fast stream has a declining N_P and T_P, and $|\mathbf{B}|$ mimics P_t. β fluctuates greatly in the interaction region.

Over about four hours before the SI, B_x/B, B_y/B, and B_z/B are relatively quiet, respectively staying negative, positive, and positive, for hours. But within the following four hours, B_x/B changes from negative to positive, and then fluctuates back and forth frequently; B_y/B changes from positive to negative; and B_z/B varies from positive to negative, and back to positive quickly. At about 4:30 UT, quite close to the SI, B_y/B and B_z/B change polarities again, sharply and simultaneously.

We believe the above behavior of the magnetic field is associated with a nearby sector boundary and is also affected by an ICME-like structure ahead. The variation of the magnetic field direction between dashed lines *a* and *b* is much less sinusoidal than what we would expect for a typical magnetic cloud. Moreover, the very noisy fluctuations of the magnetic field closely after the interface and an increasing speed profile mark this as an SIR. Our identification is confirmed by the absence of a halo CME within nine days before the occurrence of this event from the Large Angle and Spectrometric Coronagraph (LASCO) (Brueckner *et al.*, 1995) CME catalogue (*http://cdaw.gsfc.nasa.gov/CME_list/*).

For this event, assuming that the wave propagates perpendicularly to the magnetic field, we find the fast magnetoacoustic wave speed to be 63 km s^{-1} at 00:33 UT on May 18, and 82 km s^{-1} at 19:48 UT on the same day. Using the shock-coplanarity assumption and tangential-discontinuity normal, respectively, we can get the normal direction to the interface, and then calculate the normal solar-wind velocity jump of 116 km s^{-1} at 00:33 UT and of 100 km s^{-1} at 19:48 UT. So the fast Mach numbers are respectively 1.84 and 1.23, at the two discontinuities. These pressure jumps are indeed consistent with being a forward – reverse shock pair.

Again, the low-speed side of the interface is poorly correlated between magnetic field, density, and temperature, even ignoring the obvious shock-heating spike. The high-speed side shows at least qualitative correlation. Once again it appears that the structure in the slow stream is imposed at the source while the structure in the fast stream is more consistent with the compression of an originally more uniform region.

The plasma heating at the two shocks is quite evident here and can be used to estimate how long before the shocks formed. The leading (forward) shock has been acting on the plasma for some time although it was weaker earlier, judging from the temperature profile that decreases smoothly as the interface is reached. The trailing (reverse) shock is weaker than the leading shock, and makes a thin region of enhanced temperature, suggesting that the shock only recently formed.

6. Shock-Association Rate of SIRs during the Period 1995 – 2004

Solar cycle 23 started in May 1996 when the monthly sunspot number (SSN) reached a low of 8.0 and reached a maximum in April 2000 of 120.8. Rather than confining our study to only solar cycle 23, we use all the data available from *Wind* that includes one and a half years of data in 1995 and 1996 from solar cycle 22. With the *Wind* and ACE data, we have identified 365 SIRs in all, 196 of them being CIRs. Excluding data gaps and noisy data, the average annual SIR event number is about 37.

From the observations by *Ulysses*, *Pioneer*, and *Voyager*, we know that shocks typically form beyond ∼ three AU due to the steepening of quasi-stationary, fast solar-wind streams (*e.g.*, Gosling, Hundhausen, and Bame, 1976; Hundhausen and Gosling, 1976; Smith and Wolfe, 1976; Gosling *et al.*, 1993). Few CIRs are revealed bounded by shocks at one AU (*e.g.*, Gosling *et al.*, 1972; Ogilvie, 1972). Reverse shocks have been observed at one AU associated with fast streams in the absence of associated forward shocks (Formisano and Chao, 1972; Burlaga, 1974; Gosling *et al.*, 1978). However, the above claim is mostly based on observations around the early 1970s. It is possible that the relatively low quality of the early data set has allowed some shocks to be missed, although some prominent fast shocks with ICMEs and reverse shocks associated with SIRs were reported. In addition, the earlier literature was based on studies covering a part of solar cycle 20, and some discrepancy may arise between our study and the earlier work, because the solar-activity strength may differ from solar cycle to solar cycle.

In this analysis, where we quantify these statistics, we find that 88 SIRs are associated with shock(s) among the 365 SIRs observed over the ten years, *i.e.* that the SIR shock-association rate is 24% at one AU. Excluding the 41 hybrid events, among the remaining 324 "pure" SIRs, 68 events have shocks, for a 21% occurrence. There are 60 CIRs with shocks, or in other words, 31% of all CIRs. Though it is well known that shocks can form with SIRs within one AU (*e.g.*, Gosling *et al.*, 1978), this is still an unexpectedly large number. The shock-association rate is higher for CIRs than SIRs, partially due to the stronger stream interaction in CIRs, which is, in turn, caused by the usually faster and larger streams in CIRs, as documented in our survey.

Moreover, some events are associated with more than one shock, especially for hybrid events consisting of complex solar-wind structure. Though in some events, there are two or more forward shocks occurring with one SIR, we only count leading shocks once in this study. If the two or more forward shocks are associated with one reverse shock, we only count it as one pair of forward – reverse shocks, and do not count it again as one event with only a forward shock. We have not found any events associated with two or more reverse shocks. We recall that the current solar-activity strength may differ from that of solar cycle 20 when the early observations are conducted.

Table I gives the yearly numbers and percentages of SIRs, CIRs, SIRs with shocks, SIRs with only forward shock(s), or only a reverse shock, or with a forward – reverse shock pair. In all, among the 88 SIRs with shocks, 62 SIRs, *i.e.* 70% are associated with only a forward shock, while another 21 events, *i.e.* 24%, occur with only a reverse shock. That is, more than twice as many SIRs are associated with forward shocks than with reverse shocks. Among the 60 shocks associated with CIRs, 61% have only a forward shock, while 31% have only a reverse shock.

Following Gosling and Pizzo (1999), the forward shocks propagate antisunward, westward, and equatorward, while the reverse shocks propagate sunward, eastward, and poleward in both hemispheres. The *Wind* and ACE spacecraft are both near the ecliptic plane, so we expect to see more forward shocks than reverse ones at one AU if both types of shocks form near one AU, and we do. This observation is therefore consistent with the expected configuration of the stream interaction deflections. As the observation point moves outward, if the two types of shocks bounding SIRs are well formed, we might observe more reverse shocks than forward shocks. However, where and when the forward and reverse shocks form is still an open issue.

Our preponderance of forward shocks is controversial because before this study conventional wisdom, derived from SIR modeling (J.T. Gosling, private communication, 2005), had suggested that the forward and reverse shocks form at about the same time but at different distances from the Sun. Thus, SIR-associated reverse shocks would have to form closer to the Sun than forward shocks, leading us to expect to see more reverse shocks than forward shocks in the shock-growth region at one AU.

Hundhausen's (1973) 1-D gas-dynamic simulation appears to suggest that the forward shocks are formed farther away from the Sun than reverse shocks, albeit the spacing between the illustrated time steps in this simulation is large. In addition, Hu's (1993) MHD model, as an example, has a reverse shock that emerges at 1.03 AU and becomes fully developed near 1.6 AU; while the forward shock occurs later at a farther distance from the Sun (1.3 AU) and becomes fully developed near 1.8 AU, eventually becoming stronger than the reverse shock. Such simulations are challenged by our observational results.

The three columns (dark gray, white, light gray) in Figure 4, respectively, show the solar-cycle variation of occurrence rates of SIRs with only a forward shock, with only a reverse shock, and with a pair of forward – reverse shocks, among all SIRs over the ten years. The sum of the three is the SIR shock-association rate. Every year, the fraction of SIRs with only forward shocks is larger than the one with only reverse shocks. For the precise number, see Table I.

TABLE I

Occurrence rates of SIRs, CIRs, and shocks bounding SIRs.

Year	1995	1996	1997	1998	1999	2000	2001	2002	2003	2004	All
SIR No.	35	34	36	33	36	32	32	41	45	41	365
CIR No.	20	17	15	18	23	18	18	20	25	22	196
CIRs fraction among SIRs	57.14	50.00	41.67	54.55	63.89	56.25	56.25	48.78	55.56	53.66	53.70
No. of SIR with shock(s)	11	6	11	13	13	6	12	10	4	2	88
No. with only forward shock	8	5	10	8	9	4	8	6	3	1	62
No. with only reverse shock	3	1	1	4	2	2	3	3	1	1	21
No. with a pair of forward – reverse shocks				1	2		1	1			5
Of all SIRs											
% with shock(s)	31.43	17.65	30.56	39.39	36.11	18.75	37.50	24.39	8.89	4.88	24.11
% with only forward shock	22.86	14.71	27.78	24.24	25.00	12.50	25.00	14.63	6.67	2.44	16.99
% with only reverse shock	8.57	2.94	2.78	12.12	5.56	6.25	9.38	7.32	2.22	2.44	5.75
% with a pair of forward – reverse shocks				3.03	5.56		0.03	2.44			1.37
Of SIRs with shock(s)											
% with only forward shock	72.73	83.33	90.91	61.54	69.23	66.67	66.67	60.00	75.00	50.00	70.45
% with only reverse shock	27.27	16.67	9.09	30.77	15.38	33.33	25.00	30.00	25.00	50.00	23.86
% with a pair of forward – reverse shocks				7.69	15.38		0.08	10.00			5.68

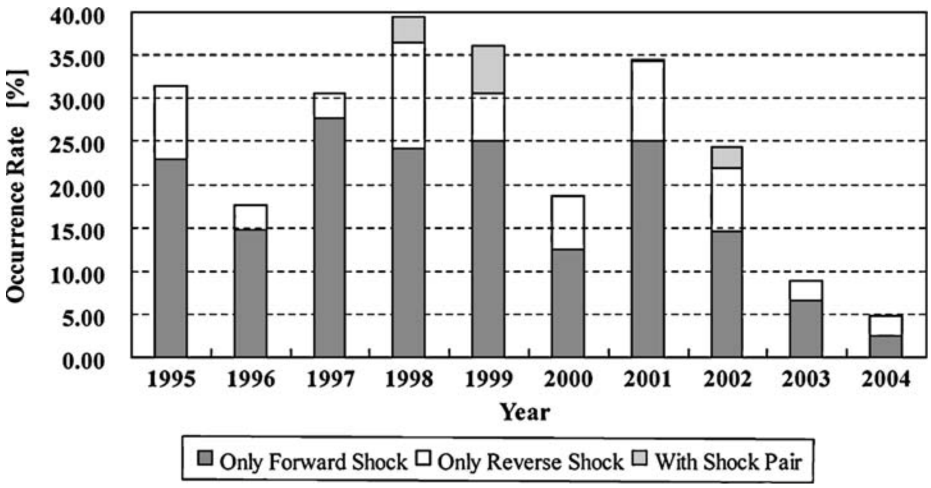

Figure 4. Occurrence rates of SIRs with shocks.

The SIR shock-association rate roughly increases with solar activity, except for 1998 and 2000. It reaches the maximum, 39%, in 1998. And it is as low as 19% in 2000. The minimum appears in 2004: ∼5%. But the SIR association rate with only forward shocks has no clear trend over the ten years.

In contrast, from a survey of *Pioneer Venus Orbiter* (PVO) solar-wind data at 0.72 AU during 1979 – 1988, Lindsay *et al.* (1994) found that only 10% of stream interactions produced interplanetary shocks (without forward or reverse specified therein) during the declining phase of the solar cycle, while no stream interactions produced shocks near solar minimum. The small number of cases of interplanetary shocks (six) associated with stream interactions results in some statistical uncertainty in their estimate. Though the studies are conducted over different solar cycles, the comparison between our survey with their study suggests that many of the shocks form in the region from 0.72 AU to 1.0 AU.

Another approach is to calculate the expected Mach number on either side of the SIR. Assuming the wave propagates perpendicular to **B**, the fast magnetoacoustic wave speed is $(V_A^2 + C_s^2)^{1/2}$. The density (N_P) is higher in the acceleration phase of a slow stream (indicated by 1) than in the deceleration phase of a fast stream (indicated by 2); while the plasma temperature (T_1) is lower than T_2. Thus the magnetoacoustic wave speed (V_{MA1}), is smaller than V_{MA2}. Therefore, for the same change of velocity along the SI normal, it would be easier to produce a Mach number larger than one in the acceleration region of the slow stream than in the deceleration region of the fast stream. Again, this line of reasoning is consistent with our observations.

Of the 365 SIRs, only five events (1%) are associated with a pair of forward – reverse shocks. One of them is a hybrid event in 2001, and the other four are all CIRs. It is very rare for spacecraft to observe shock pairs with SIRs at one AU. In contrast, at distance greater than about two to three AU and at low heliographic latitudes, CIRs and presumably most SIRs, are commonly bounded by forward – reverse shock pairs (*e.g.*, Gosling and Pizzo, 1999), *e.g.*, during *Ulysses*' second polar orbit, about half of the well-defined SIRs observed poleward of S9.8° were bounded by forward – reverse shock pairs (Gosling *et al.*, 2001).

In addition, averaged over the SIRs having reverse shocks, these shocks occur 13 hours later than the stream interface, consistent with the MHD simulation of Pizzo (1989) and Hu (1993). They concluded that the shocks form at an angle of 7 – 10° in heliocentric azimuth on either side of the stream interface, which corresponds to 12 – 17 hours in corotation time. From the survey, the average decrease of P_t is 61 pPa across the reverse shock.

7. Properties of Stream Interaction Regions

Table II lists the annual averages of seven parameters (duration, R_D, size, P_{max}, B_{max}, R_V, and ΔV) as well as their probable errors of the mean, indicated in parentheses. The last three rows in this table provide the corresponding averages as well as their probable errors of the mean, the maximum, and the minimum, based on all the 365 SIRs. The five panels in Figure 5 respectively show the solar-cycle variations of annual number of SIRs, size, P_{max}, B_{max}, and ΔV of SIRs from 1995 to 2004, with the error bars presenting the corresponding probable errors of the mean in each year. We see that P_{max} and ΔV vary up to about 1.5 times the minima, but none of these five parameters changes as much as those of ICMEs (Jian *et al.*, 2006) over the ten years.

During the declining phase of solar cycle 23, there are a few more SIRs than at other times, with a maximum occurrence of 45 events in 2003; the second highest value (41), occurs in both 2002 and 2004. The fewest (32), occurs in 2000 and 2001, around solar maximum. Thus the SIR occurrence rate changes with the variation in the solar magnetic configuration during the period under study, although to a much smaller extent than ICMEs. This change is somewhat out of phase with the ICME occurrence-rate variation.

From Table I, we can see that the CIR occurrence rate has no simple solar-cycle dependence, except for being roughly larger in the descending phase. In 1999, the occurrence rate of CIRs (64%) is slightly higher; but we are aware of some uncertainty caused by identification errors, data gaps, or changes in viewing location, *etc.*, so the high CIRs fraction in 1999 is not necessarily statistically significant.

Similarly, for the inner heliosphere, Lindsay *et al.* (1994) found that the stream-interaction occurrence observed at 0.72 AU varied out of phase with the solar cycle, with an average of about 31 prior to solar maximum (1986 – 1987), and of only about 16 around the maximum of solar cycle 21 (1979 – 1981). The SIRs occurrence rate at 0.72 AU changes more over 1979 – 1988 than we found in solar cycle 23 possibly because of their emphasis on CIRs.

Averaged over all 365 events, SIR events last 36.7 ± 0.9 hours, and the duration before the peak is about 1.21 ± 0.07 times larger than that after. This observation is consistent with similar geometries on either side of the interface considering

TABLE II
SIR statistics.

Year	⟨Duration⟩ ($\delta^a D$) [hr]	$\langle R_D = D_{before} / D_{after} \rangle$ (δR_D)	⟨Size⟩ (δS) [AU]	$\langle P_{max} \rangle$ (δP_{max}) [pPa]	$\langle B_{max} \rangle$ (δB_{max}) [nT]	$\langle R_V = V_{max} / V_{min} \rangle$ (δR_V)	$\langle \Delta V \rangle$ ($\delta \Delta V$) [km s^{-1}]
1995	37.24 (2.95)	1.03 (0.17)	0.40 (0.03)	229.86 (22.00)	17.36 (0.97)	1.81 (0.06)	262.06 (18.14)
1996	35.82 (2.92)	0.92 (0.12)	0.37 (0.03)	130.85 (8.44)	12.90 (0.48)	1.55 (0.02)	192.71 (9.32)
1997	26.97 (1.85)	1.26 (0.22)	0.27 (0.02)	145.86 (12.77)	13.16 (0.57)	1.49 (0.03)	164.61 (9.15)
1998	43.15 (2.99)	1.16 (0.16)	0.46 (0.03)	169.15 (12.73)	15.63 (0.63)	1.67 (0.05)	220.97 (14.81)
1999	38.30 (3.06)	0.95 (0.15)	0.43 (0.03)	209.92 (19.19)	17.55 (1.08)	1.74 (0.06)	251.19 (17.93)
2000	32.48 (2.04)	1.46 (0.24)	0.37 (0.02)	198.09 (28.43)	16.30 (1.03)	1.72 (0.05)	249.53 (17.80)
2001	34.60 (3.10)	1.03 (0.18)	0.38 (0.03)	170.47 (16.12)	15.59 (0.76)	1.66 (0.05)	221.38 (13.11)
2002	35.74 (2.05)	1.60 (0.34)	0.40 (0.02)	214.78 (22.01)	16.82 (0.92)	1.68 (0.05)	234.51 (16.63)
2003	37.64 (2.67)	0.99 (0.12)	0.49 (0.04)	167.00 (13.45)	15.67 (0.61)	1.67 (0.04)	263.80 (12.89)
2004	44.08 (3.30)	1.59 (0.36)	0.49 (0.04)	129.78 (7.18)	13.73 (0.53)	1.65 (0.05)	229.02 (14.85)
All	36.73 (0.89)	1.21 (0.07)	0.41 (0.01)	176.22 (5.63)	15.47 (0.26)	1.66 (0.02)	229.95 (4.89)
Max	92.00	13.23	1.24	850	41.0	2.96	603
Min	6.75	0.05	0.06	52	7.2	1.17	61

[a] δ presents the probable error of the mean for the corresponding parameter.

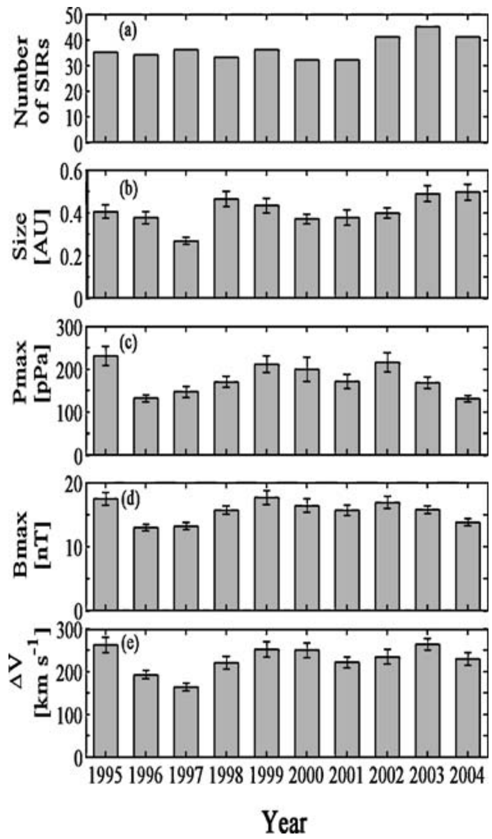

Figure 5. Annual statistics of some properties of SIRs during the period 1995 – 2004. (a) Occurrence rates of SIRs. (b) Scale size of each SIR. (c) Peak pressure. (d) Maximum magnetic field. (e) Change in the solar-wind velocity from slow stream to fast stream. The probable error of the mean is shown.

the different velocities on the two sides. The scale size of SIRs varies from 0.06 to 1.24 AU, with a mean of 0.41 ± 0.01 AU, the same scale of our ICME events (Jian *et al.*, 2006). It is largest in 2003 and 2004, during the declining phase of the solar cycle.

The average P_{max} of SIRs is 176 ± 6 pPa, a smaller value than that of ICMEs, suggesting that the average strength of stream interaction is weaker than the interaction of ICMEs with ambient solar wind at one AU. The P_{max} apparently declines from 2002 to 2004, meaning that the interaction weakens as the solar activity declines. Over the ten years, B_{max} has a variation similar to P_{max}, with an average of 15.5 ± 0.3 nT.

Since annual averages of R_V and ΔV have similar solar-cycle variations, we only show the latter in Figure 5. They have no clear solar-cycle dependence, reaching maxima in 2003. They both reach a minimum in 1997, just after the SSN minimum, but can reach high values around solar maximum and in the solar-cycle declining phase. This behavior may be attributed to the fact that over the ten years, V_{min} is almost constant, while V_{max} varies greatly.

In 2001, all five parameters in Figure 5 are relatively low. Near solar minimum, we are presumably seeing the equatorial extent of the large polar coronal holes. While around solar maximum, it is likely that we are observing smaller coronal holes, which may also occur at lower latitudes. Certainly, the solar-wind speed has been found to be a function of coronal hole size, so it makes sense that pressure and magnetic field might be too (*e.g.*, Nolte *et al.*, 1976; McComas, Elliott, and von Steiger, 2002). Our result partially represents the properties of the plasma originating from the two kinds of coronal holes. On average, $V_{\rm max}$ is 1.66 ± 0.02 times $V_{\rm min}$, and the former is 230 ± 5 km s^{-1} larger than the latter. The values of $R_{\rm V}$ and ΔV are both larger than those of ICMEs, consistent with the SIR's role in the interaction of fast streams with slow streams.

The two panels in Figure 6 individually show the probability distributions of $P_{\rm max}$ and ΔV, one on a quasi-logarithmic scale (the bin values are successively raised by the power 1.06 to distribute the data well across the bins), and the other on a linear scale. Roughly, they are all centrally distributed. The $P_{\rm max}$ varies from 52 to 850 pPa, and is distributed mostly around 140 pPa, where about 24% of SIRs fall. The velocity change varies from 61 to 603 km s^{-1}, centered on 200 km s^{-1}, and approximately 22% of the 365 SIRs have a ΔV between 175 and 225 km s^{-1}.

8. Summary

Total perpendicular pressure ($P_{\rm t}$) can assist in the identification of different interaction types. A pressure peak with gradual slopes on both sides is the characteristic feature of the stream interaction region (SIR). From 1995 to 2004, *Wind* and ACE observed 365 SIRs in all, 54% of them being CIRs. The SIR occurrence rate has little solar-cycle dependence. The CIR occurrence rate varies more with solar cycle than the SIR rate, from 15 in 1997 up to 25 in 2003. Due to other temporal variations in the solar wind, such as ICMEs, and partially because of data gaps, on average we can only detect 1.7 CIRs per Carrington rotation.

On average about 24% of SIRs are associated with shocks, and around 31% of CIRs occur with shocks. Among the SIRs with shocks, 70% have only forward shocks, and 24% have only reverse shocks. Hence, at one AU, only about 1% of all SIRs occur with a pair of forward-reverse shocks. The SIR shock-association rate is much larger than the rate found by Lindsay *et al.* (1994) based on PVO data at 0.72 AU, suggesting that some forward or reverse waves bounding the interaction region may have steepened into shocks from 0.72 to 1.0 AU.

Defining the stream interface where the $P_{\rm t}$ reaches the maximum, the average duration of an SIR at one AU is 36.7 ± 0.9 hours, and the leading portion of the interaction before the interface lasts about 1.21 ± 0.07 times longer than the trailing portion, indicating a temporal asymmetry. In addition, the average scale size of SIR is 0.41 ± 0.01 AU, as large as ICMEs; peak pressure ($P_{\rm max}$) is 176 ± 6 pPa, and the average ΔV is 230 ± 5 km s^{-1}. In contrast, the CIRs last 36.8 ± 1.2 hours, with a size of 0.44 ± 0.02 AU, a $P_{\rm max}$ of 214 ± 9 pPa, and a ΔV as high as 285 ± 6 km s^{-1}.

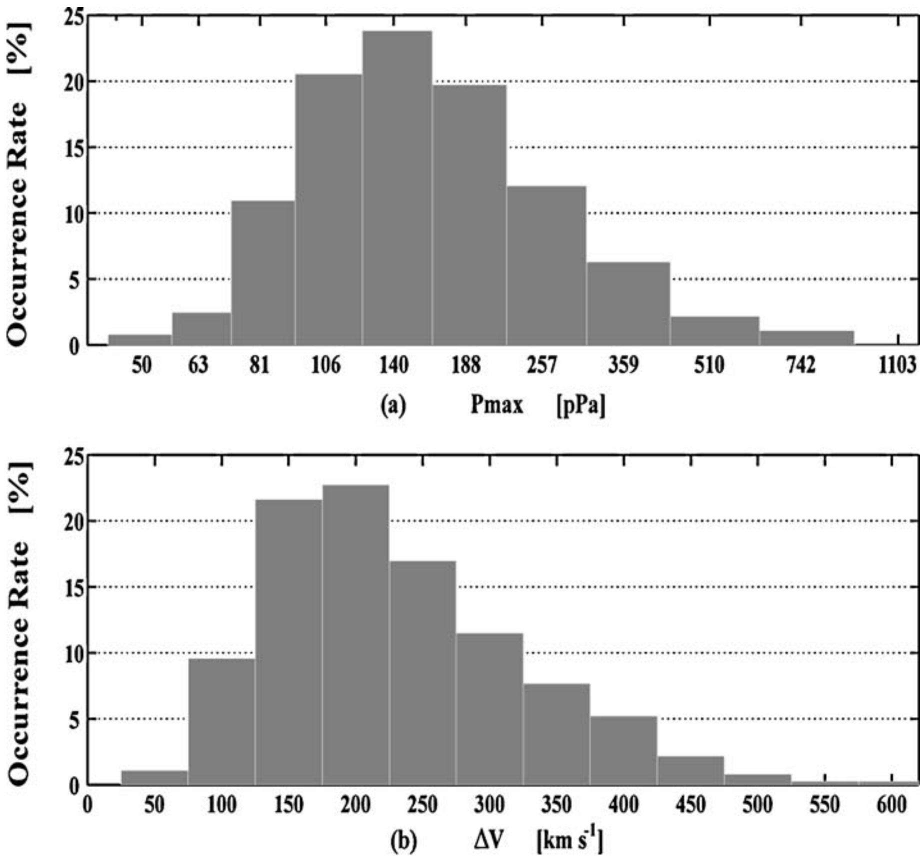

Figure 6. Probability distribution: P_{max} and ΔV of SIRs (1995 – 2004).

The CIRs are typically larger and stronger SIRs. Our statistics should also provide some needed guidance for simulation work on stream interactions.

The properties (size, P_{max}, B_{max}, R_V, ΔV, *etc.*) of SIRs have no simple solar-cycle dependence. They reach low values around solar maximum, probably because around solar minimum, a larger fraction of fast streams emanate from the high-heliolatitude coronal holes, and the properties of such fast streams differ from the ones originating in the low-heliolatitude coronal holes near solar maximum. The solar-cycle variations of the CIRs properties mimic those of SIRs, except that CIRs often last longer, and have stronger interactions. This demonstrates that SIRs and CIRs involve the same physical mechanisms, with the only exception being that SIRs have low recurrence.

Since single-point observations are definitely not sufficient to study the temporal and spatial evolution of stream interactions, the launch of the *Solar-Terrestrial Relations Observatory* (STEREO), will add two more observation points on either side of the *Wind*/ACE pair, enabling stream interaction to be probed only a day or so apart, and determine how steady SIRs are, especially their forward and reverse shocks.

Appendix: List of stream interaction regions (SIRs) from *Wind* and ACE data during 1995 – 2004

SIR #	CIR #	Start UT [mm/dd hhmm]	End UT [mm/dd hhmm]	Discontinuity UT [mm/dd hhmm]	F/R[a] Shock	ΔP^b (pPa)		Stream interface (SI) UT [mm/dd hhmm]	P_{max} (pPa)	V_{max} (km s^{-1})	V_{min} (km s^{-1})	ΔV^c (km s^{-1})	B_{max} (nT)	Comments
1995														
1	1	01/01 1937	01/03 2000	01/01 1937	F	33 → 88	55	01/02 0556	173	720	320	400	16.3	P_t plateau-like and irregular
2	2	01/17 0200	01/18 2000	01/17 1918	/	125 → 160	35	01/17 2323	240	536	330	206	19	
3		01/22 0400	01/23 0200					01/22 1300	110	435	335	100	11	
4	3	01/28 1800	01/30 1100	01/30 1000	/	85 → 47	−38	01/29 1520	290	747	290	457	20.5	P_t zigzag
5	4	02/10 2200	02/13 1400					02/11 0600	170	710	330	380	14	P_t irregular
6	5	02/25 2000	02/28 2000	02/26 0256	F	90 → 130	40	02/26 0325	180	640	262	378	14.6	Long-time plateau after P_{max}
				02/26 0718	/	150 → 112	−38							
7*	6	03/25 2200	03/27 2100					03/26 1013	207	520	290	230	18.5	After an ICME[d]
8*	7	04/06 1100	04/07 2200	04/07 2025	R	110 → 28	−82	04/07 1240	580	763	300	463	28	Catching up with an ICME-like structure
9		04/22 0200	04/25 0400					04/22 1823	130	510	300	210	13	P_t plateau-like
10	8	04/26 0800	04/27 0900					04/26 2110	250	720	420	300	17.6	
11	9	05/01 2000	05/03 0030	05/02 2357	/	90 → 50	−40	05/02 0350	240	745	360	385	17	A trough of P_t, two steps

(*Continued on next page*)

(*Continued*)

SIR #	CIR #	Start UT [mm/dd hhmm]	End UT [mm/dd hhmm]	Discontinuity UT [mm/dd hhmm]	F/R[a] Shock	ΔP^{b} (pPa)		Stream interface (SI) UT [mm/dd hhmm]	P_{max} (pPa)	V_{max} ($km\,s^{-1}$)	V_{min} ($km\,s^{-1}$)	ΔV^{c} ($km\,s^{-1}$)	B_{max} (nT)	Comments
12*		05/15 1700	05/16 2200					05/16 0542	300	520	310	210	25	Containing an ICME
13	10	05/23 0300	05/24 0600	05/24 0440	/	110 → 60	−50	05/24 0045	230	680	330	350	17	
14	11	05/29 0300	05/31 0600					05/30 0638	225	700	380	320	19.8	P_t irregular
15		06/09 0000	06/10 2200					06/10 0745	100	420	295	125	13	P_t irregular
16	12	06/19 0000	06/19 2000	06/19 1330	/	200 → 80	−120	06/19 1230	440	740	340	400	25	P_t noisy
17	13	06/25 0600	06/26 0343	06/26 0343	R	73 → 32	−41	06/25 2327	180	570	373	197	15.7	Two peaks of P_t, trough
18		07/12 0900	07/14 0000					07/13 0200	110	326	265	61	12	
19	14	07/16 0918	07/17 0400	07/16 0918	/	40 → 66	26	07/16 2105	260	690	358	332	20	
20		07/24 0223	07/25 1000	07/24 0223	F	24 → 87	63	07/24 0923	180	510	318	192	19.4	Some rotations of **B**
21		08/07 0905	08/09 1000	08/07 0905	/	35 → 78	43	08/07 1240	140	620	340	280	12	P_t irregular, several peaks
				08/07 1407	/	110 → 63	−47							
22	15	08/13 1300	08/14 1800					08/14 0308	90	660	360	300	11.2	Weak, T_P not high
23		08/24 2212	08/25 1100	08/24 2212	F	65 → 130	65	08/25 0105	220	446	318	128	14.6	
24	16	09/05 0800	09/06 0500	09/06 0230	R	150 → 68	−82	09/05 1920	320	630	310	320	21	
25		09/10 1230	09/11 0600					09/10 1820	140	580	397	183	13.2	
26		10/01 2000	10/03 1200					10/02 1341	155	490	300	190	12	Followed by a strong SIR

(*Continued on next page*)

(*Continued*)

SIR #	CIR #	Start UT [mm/dd hhmm]	End UT [mm/dd hhmm]	Discontinuity UT [mm/dd hhmm]	F/R[a] Shock	ΔP^b (pPa)		Stream interface (SI) UT [mm/dd hhmm]	P_{max} (pPa)	V_{max} (km s^{-1})	V_{min} (km s^{-1})	ΔV^c (km s^{-1})	B_{max} (nT)	Comments
27	17	10/04 0000	10/04 2030	10/04 1943	/	57 → 30	−27	10/04 0740	400	720	383	337	22	15-min extremely high P_t
28*		10/18 1042	10/20 1400	10/18 1042	F	30 → 200	170	10/19 1823	410	578	300	278	29	Containing an ICME
				10/18 1900	/	226 → 182	−44							
				10/19 1751	F	200 → 360	160							
29	18	10/30 0100	11/01 1800	10/30 0927	F	42 → 65	23	10/30 1322	108	640	300	340	13	P_t irregular, plateau
30		11/04 0800	11/06 0600					11/05 1430	162	610	380	230	15	
31		11/21 1600	11/24 0000					11/22 0720	72	367	303	64	7.2	Weak, T_P not high
32	19	11/27 0000	11/27 2000					11/27 1120	530	526	260	266	30	Quite classic slow stream
33*		12/15 0437	12/17 1800	12/15 0437	F	38 → 88	50	12/15 1425	123	440	310	130	12.5	ICME in SIR
				12/15 1457	/	110 → 80	−30							
				12/16 0450	/	93 → 68	−25							
34	20	12/24 0600	12/24 1600	12/24 0600	F	53 → 210	157	12/24 0835	470	580	330	250	27	One reverse shock at 12/25 2305
				12/24 0845	/	470 → 265	−205							
35		12/31 0000	12/31 2100					12/31 0620	110	510	330	180	11.6	V_P does not monotonically increase

(*Continued on next page*)

(*Continued*)

SIR #	CIR #	Start UT [mm/dd hhmm]	End UT [mm/dd hhmm]	Discontinuity UT [mm/dd hhmm]	F/R[a] Shock	ΔP^{b} (pPa)		Stream interface (SI) UT [mm/dd hhmm]	P_{max} (pPa)	V_{max} (km s^{-1})	V_{min} (km s^{-1})	ΔV^{c} (km s^{-1})	B_{max} (nT)	Comments
1996														
1	1	01/02 1400	01/03 1200					01/02 1929	90	570	370	200	11.5	Little heating of plasma
2	2	01/14 1000	01/15 0000					01/14 1701	250	640	370	270	18	
3		01/19 1400	01/21 0200					01/19 2235	120	530	385	145	12	Irregular P_t
4	3	02/10 0120	02/11 2000	02/10 0120	/	34 → 42	8	02/11 0525	160	630	340	290	13	
				02/11 0820	/	90 → 50	−40							
5		03/02 0400	03/04 2000	03/02 2032	F	36 → 47	11	03/03 0300	110	490	305	185	9.5	
6	4	03/20 0000	03/22 0000					03/20 2012	130	650	400	250	11	Irregular P_t
7		04/07 2000	04/09 1700	04/08 0241	F	47 → 100	53	04/08 1339	105	500	290	210	11	
				04/08 1310	F	55 → 100	45							
8		05/18 2000	05/21 1000					05/20 0100	66	485	310	175	9.5	No sharp T_P increase, small peaks of P_t
9*		05/28 2200	05/30 0500					05/29 0140	200	470	340	130	16.5	Following an ICME
10		06/05 1400	06/06 1800					06/06 0400	135	480	320	160	14.5	
11		06/14 1800	06/16 1200	06/16 0419	/	95 → 57	−38	06/15 1345	80	425	290	135	10.3	P_t plateau, N_P and T_P do not change exactly simultaneously

(*Continued on next page*)

(*Continued*)

SIR #	CIR #	Start UT [mm/dd hhmm]	End UT [mm/dd hhmm]	Discontinuity UT [mm/dd hhmm]	F/R[a] Shock	ΔP^b (pPa)		Stream interface (SI) UT [mm/dd hhmm]	P_{max} (pPa)	V_{max} (km s^{-1})	V_{min} (km s^{-1})	ΔV^c (km s^{-1})	B_{max} (nT)	Comments
12		06/18 2000	06/19 1000	06/18 2236	F	65 → 82	17	06/19 0145	280	550	380	170	19	
				06/19 0157	/	260 → 160	−100							
13*	5	07/01 1220	07/04 0200	07/01 1220	/	20 → 40	20	07/02 0420	110	550	320	230	14	Containing an ICME
				07/01 1417	/	63 → 85	22							
14		07/11 0600	07/13 1800					07/13 0000	80	440	300	140	11.5	P_t plateau, maybe a recurrence of event 11, but fast stream with not quite high speed
15		07/28 0800	07/29 1800	07/28 1215	F	45 → 90	45	07/28 1415	110	395	305	90	12.3	
				07/28 1747	/	92 → 77	−15							
16	6	07/30 1500	07/31 1200					07/31 0240	170	580	360	220	15	
17		08/08 0000	08/10 1200					08/09 0800	80	415	330	85	9	
18		08/14 0000	08/15 0600					08/14 0930	90	540	360	180	10.3	
19	7	08/16 0200	08/17 1200	08/16 0745	F	55 → 105	50	08/16 0755	110	590	370	220	11	
20		08/22 1310	08/23 1800	08/22 1310	/	17 → 34	17	08/23 0425	130	532	360	172	11.8	
21	8	08/28 1500	08/29 1500					08/29 0140	150	620	380	240	13.6	No sharp T_P increase
22		09/03 1800	09/07 0000					09/04 2300	70	440	310	130	10.5	

(*Continued on next page*)

(*Continued*)

SIR #	CIR #	Start UT [mm/dd hhmm]	End UT [mm/dd hhmm]	Discontinuity UT [mm/dd hhmm]	F/R[a] Shock	ΔP^{b} (pPa)		Stream interface (SI) UT [mm/dd hhmm]	P_{max} (pPa)	V_{max} (km s^{-1})	V_{min} (km s^{-1})	ΔV^{c} (km s^{-1})	B_{max} (nT)	Comments
23	9	09/19 0400	09/20 2200					09/19 1645	100	690	450	240	11	
24	10	09/26 1400	09/26 2200	09/26 2136	R	$70 \rightarrow 20$	−50	09/26 1830	200	685	440	245	18.6	
25	11	10/01 1800	10/03 0000					10/02 1255	180	560	330	230	17.5	
26		10/08 1200	10/09 1600					10/09 0500	130	540	350	190	12.5	P_t and V_P irregular
27	12	10/17 1400	10/18 0900					10/17 2238	115	615	390	225	12	
28	13	10/21 2000	10/23 0800					10/23 0000	150	700	390	310	14.5	
29	14	10/27 2000	10/28 1200					10/28 0300	150	620	370	250	14.8	
30		11/03 1200	11/04 1800	11/03 2300	/	$50 \rightarrow 110$	60	11/04 0000	123	450	320	130	12.3	
				11/04 0205	/	$105 \rightarrow 80$	−25							
31	15	11/13 1250	11/14 1200	11/13 1250	/	$32 \rightarrow 54$	22	11/13 2105	125	500	365	135	14.6	
32	16	11/24 0000	11/25 0600					11/24 0830	125	480	310	170	11.5	Followed by long V_P increase
33	17	12/09 1600	12/10 1200	12/09 1850	/	$60 \rightarrow 90$	30	12/09 2310	160	550	350	200	16	Irregular T_P and P_t
34		12/14 0817	12/16 1557					12/15 1600	65	580	380	200	8.5	
1997														
1		01/06 1800	01/07 1600					01/07 0150	110	460	346	114	11	Two peaks of P_t
2*	1	01/10 0052	01/11 0900	01/10 0052	F	$15 \rightarrow 65$	50	01/11 0200	500	590	375	215	24.2	ICME + SIR
3	2	01/25 1830	01/26 1730					01/26 1000	215	600	320	280	18	A trough of P_t

(*Continued on next page*)

(*Continued*)

SIR #	CIR #	Start UT [mm/dd hhmm]	End UT [mm/dd hhmm]	Discontinuity UT [mm/dd hhmm]	F/R[a] Shock	ΔP^{b} (pPa)		Stream interface (SI) UT [mm/dd hhmm]	P_{max} (pPa)	V_{max} (km s^{-1})	V_{min} (km s^{-1})	ΔV^{c} (km s^{-1})	B_{max} (nT)	Comments
4		01/27 1200	01/28 1300	01/28 0854	R	80 → 37	−43	01/28 0855	120	685	460	225	12	Weak, near contact with previous SIR
5		02/05 0300	02/06 2000					02/05 2100	95	470	315	155	11.5	
6	3	02/08 0820	02/08 1740	02/08 1327	/	200 → 120	−80	02/08 1313	233	600	380	220	16	Relatively neat, short
7*		02/17 0300	02/18 0600					02/17 1743	110	435	320	115	12.8	V_P does not increase monotonically, containing an ICME
8		02/20 1800	02/22 0100					02/21 0820	120	435	320	115	11	Followed by another V_P enhancement
9	4	02/27 1729	02/28 1200	02/27 1729	F	13 → 26	13	02/28 0050	165	630	440	190	16.5	V_P increases in two steps
10		03/05 1255	03/06 0400	03/05 1255	F	37 → 80	43	03/05 1547	130	425	320	105	11.7	Short
11	5	03/11 2000	03/12 1600					03/12 0210	215	525	295	230	13.5	Noisy plateau of P_t after the P_t peak
12		03/26 0200	03/27 0000					03/26 1150	77	591	420	171	8.8	Weak

(*Continued on next page*)

(*Continued*)

SIR #	CIR #	Start UT [mm/dd hhmm]	End UT [mm/dd hhmm]	Discontinuity UT [mm/dd hhmm]	F/R[a] Shock	ΔP^{b} (pPa)		Stream interface (SI) UT [mm/dd hhmm]	P_{max} (pPa)	V_{max} (km s^{-1})	V_{min} (km s^{-1})	ΔV^{c} (km s^{-1})	B_{max} (nT)	Comments
13		03/31 1600	04/02 1000					04/01 0530	160	490	350	140	15.5	
14		04/03 1900	04/04 1400					04/04 0110	90	448	370	78	10	Closely following an SIR, interface is thick ~2 hours
15*	6	04/10 1300	04/11 0200	04/10 1300	F	70 → 120	50	04/10 2000	260	450	310	140	19.5	
16	7	04/16 0800	04/17 1400	04/16 1220	F	65 → 110	45	04/16 1700	180	550	310	240	15.5	Classic
17	8	05/01 1203	05/02 0300	05/01 1203	F	40 → 97	57	05/01 1745	170	635	330	305	16	
18		06/05 1800	06/07 2200	06/06 0953	/	95 → 60	−35	06/06 0953	95	450	320	130	9.5	Two peaks, irregular
19		06/14 1800	06/16 1100					06/15 1705	98	410	290	120	9	Weak, data gap after it
20		06/22 0000	06/23 0600	06/22 0245	/	55 → 95	40	06/22 0337	170	430	270	160	12	P_t irregular
21	9	06/27 0200	06/27 1800					06/27 1030	110	550	360	190	12.3	Neat
22		07/06 2200	07/08 0100					07/07 1605	140	455	335	120	13.5	Classic
23		07/09 0800	07/10 0600					07/09 2130	125	450	340	110	14	2-hr data gap, following a previous SIR
24		07/24 0000	07/25 0100					07/24 0550	140	480	360	120	10.7	Saw-peak
25		07/30 2000	07/31 1600					07/31 0300	165	500	305	195	17	A small trough of P_t peak

(*Continued on next page*)

(*Continued*)

SIR #	CIR #	Start UT [mm/dd hhmm]	End UT [mm/dd hhmm]	Discontinuity UT [mm/dd hhmm]	F/R[a] Shock	ΔP^{b} (pPa)		Stream interface (SI) UT [mm/dd hhmm]	P_{max} (pPa)	V_{max} (km s^{-1})	V_{min} (km s^{-1})	ΔV^{c} (km s^{-1})	B_{max} (nT)	Comments
26		08/09 0500	08/10 0300					08/09 0715	80	470	335	135	11	Irregular P_t
27	10	08/12 1600	08/14 0100					08/13 0525	76	565	350	215	8.6	Followed by another P_t peak
28	11	08/27 1200	08/28 1400					08/28 0400	110	460	300	160	14.3	Irregular P_t
29*	12	09/02 2200	09/04 0500	09/02 2238	F	$37 \rightarrow 87$	50	09/04 0007	195	570	312	258	18	Containing an ICME
				09/03 0838	F	$65 \rightarrow 120$	55							
30	13	09/26 1500	09/28 0900					09/28 0030	95	510	330	180	11.2	Weak, lasting longer before the SI
31		10/06 1800	10/08 1000					10/08 0030	95	430	315	115	10.7	Weak
32	14	10/23 0730	10/24 0130	10/23 0810	F	$32 \rightarrow 62$	30	10/23 1520	130	410	290	120	11.5	V_P does not monotonically increase, followed by another SIR
33		10/31 2300	11/01 2300	11/01 0615	F	$82 \rightarrow 132$	50	11/01 0632	150	475	325	150	13	P_t irregular
34	15	11/17 1600	11/19 0400					11/18 0625	130	505	360	145	12.8	
35		11/30 0715	11/30 1400	11/30 0715	F	$50 \rightarrow 95$	45	11/30 0750	133	460	300	160	12.3	An interpeak trough before it, short

(*Continued on next page*)

(*Continued*)

SIR #	CIR #	Start UT [mm/dd hhmm]	End UT [mm/dd hhmm]	Discontinuity UT [mm/dd hhmm]	F/R[a] Shock	ΔP^{b} (pPa)		Stream interface (SI) UT [mm/dd hhmm]	P_{max} (pPa)	V_{max} (km s^{-1})	V_{min} (km s^{-1})	ΔV^{c} (km s^{-1})	B_{max} (nT)	Comments
36		12/04 0800	12/06 1400					12/04 1902	64	415	310	105	8.7	Weak, noisy
1998														
1		01/16 0900	01/17 1200					01/16 1804	130	380	280	100	14	Classic, but not a CIR
2		01/18 0600	01/20 2000					01/19 1400	180	470	290	180	17.8	
3		01/31 1400	02/01 1500	01/31 1553	F	60 → 150	90	01/31 2345	170	480	330	150	14.5	V_P irregular, noisy, catching up with an ICME
4		02/10 1800	02/11 2300					02/11 1520	80	580	390	190	10.3	
5		02/28 0000	03/03 0000					02/28 1415	150	515	310	205	15	P_t peaks not where T_P sharply rises
6	1	03/09 2100	03/11 0400					03/10 1015	300	565	270	295	23.5	Noisy, trough in the center
7	2	03/19 2000	03/22 1200					03/21 1100	160	640	310	330	16	Three peaks of P_t
8*		03/24 1000	03/27 2300					03/26 0256	100	510	350	160	13	Containing a flux rope structure
9		04/03 2200	04/05 0600					04/04 1530	120	400	300	100	13	
10	3	04/15 1400	04/18 1522	04/18 1522	R	40 → 17	−23	04/16 2350	100	670	320	350	13	Noisy

(*Continued on next page*)

(*Continued*)

SIR #	CIR #	Start UT [mm/dd hhmm]	End UT [mm/dd hhmm]	Discontinuity UT [mm/dd hhmm]	F/R[a] Shock	ΔP^b (pPa)		Stream interface (SI) UT [mm/dd hhmm]	P_{max} (pPa)	V_{max} (km s^{-1})	V_{min} (km s^{-1})	ΔV^c (km s^{-1})	B_{max} (nT)	Comments
11		04/23 1729	04/25 0000	04/23 1729	F	50 → 150	100	04/23 2133	330	470	323	147	19.2	
				04/23 2210	/	230 → 270	40							
12	4	05/07 0800	05/08 1800	05/08 0923	F	50 → 150	100	05/08 0952	210	690	480	210	13.5	T_P increases in steps
13*	5	05/15 1353	05/17 1800	05/15 1353	F	32 → 90	58	05/16 0310	143	640	320	320	17	Two obviously different streams, containing an ICME
14	6	05/28 1400	05/30 1600	05/29 1515	F	110 → 300	190	05/29 1525	320	730	340	390	20.6	Sharp interface
15		06/03 0600	06/04 0600					06/03 1127	120	520	395	125	13	3-hr data gap
16	7	06/05 0000	06/07 1200					06/06 1920	125	660	350	310	14	A trough
17*		06/14 1400	06/16 1000					06/15 0500	90	442	312	130	12	Following an ICME
18	8	06/18 1800	06/20 1200					06/19 1300	180	520	300	220	16	P_t plateau, no sharp T_P increase
19*	9	07/04 1800	07/06 1800	07/05 0352	F	55 → 150	95	07/05 0417	200	670	400	270	14	Followed by an ICME
20*	10	07/15 1200	07/17 0024	07/17 0024	R	90 → 15	−75	07/16 0457	340	640	300	340	22.5	Two obviously different streams

(*Continued on next page*)

(*Continued*)

SIR #	CIR #	Start UT [mm/dd hhmm]	End UT [mm/dd hhmm]	Discontinuity UT [mm/dd hhmm]	F/R[a] Shock	ΔP^{b} (pPa)		Stream interface (SI) UT [mm/dd hhmm]	P_{max} (pPa)	V_{max} ($km\,s^{-1}$)	V_{min} ($km\,s^{-1}$)	ΔV^{c} ($km\,s^{-1}$)	B_{max} (nT)	Comments
21		07/20 2000	07/22 0000					07/21 0510	163	500	335	165	15.5	
22	11	07/22 1200	07/23 2000	07/23 1302	R	120 → 60	−60	07/23 0307	240	740	360	380	16.6	
23		08/05 2000	08/08 0400	08/06 0715	F	70 → 180	110	08/06 0828	225	540	350	190	22	
24	12	08/22 0000	08/23 2200	08/22 0211	F	45 → 75	30	08/22 1445	140	580	280	300	13.5	
				08/23 1023	R	80 → 40	−40							
25		09/11 0200	09/13 0800					09/12 1552	80	510	330	180	9.5	
26		09/17 1200	09/19 0800					09/18 1340	210	475	300	175	20	
27	13	10/06 1533	10/08 0000	10/06 1533	/	23 → 46	23	10/07 1630	148	600	340	260	15	ACE[e], a trough of P_t, 18-hr data gap of *Wind*
28	14	10/27 0600	10/30 0000					10/28 2100	95	630	350	280	12.5	
29	15	11/23 1000	11/24 0300					11/23 1630	150	520	310	210	16	
30		12/10 1200	12/12 1200	12/11 1934	F	60 → 120	60	12/11 2014	180	410	330	80	17.3	ACE, two peaks of P_t
31	16	12/15 1800	12/16 1100					12/16 0445	103	540	370	170	13	ACE
32	17	12/19 1200	12/21 0000					12/20 0000	80	500	340	160	11	
33	18	12/25 0200	12/26 0414	12/26 0414	R	110 → 65	−45	12/25 2000	220	540	320	220	22	
1999														
1	1	01/05 1800	01/07 1400					01/06 1421	170	575	310	265	17.2	
2	2	01/13 0800	01/15 0700	01/13 1000	F	40 → 105	65	01/13 2100	230	600	330	270	19.3	ACE, *Wind* data gaps

(*Continued on next page*)

(*Continued*)

SIR #	CIR #	Start UT [mm/dd hhmm]	End UT [mm/dd hhmm]	Discontinuity UT [mm/dd hhmm]	F/R[a] Shock	ΔP^{b} (pPa)		Stream interface (SI) UT [mm/dd hhmm]	P_{max} (pPa)	V_{max} (km s^{-1})	V_{min} (km s^{-1})	ΔV^{c} (km s^{-1})	B_{max} (nT)	Comments
3		01/26 1600	01/30 1200					01/27 1230	77	480	325	155	9	Long, weak, noisy
4	3	02/11 0749	02/12 0710	02/11 0749	F	45 → 75	30	02/11 1840	320	480	368	112	25.5	A trough of T_P, no reverse shock, ambiguous shock in *Wind* data
5		02/14 1300	02/15 1800					02/15 0125	110	678	370	308	13	P_t plateau
6	4	02/28 2144	03/02 0300	02/28 2144	F	85 → 133	48	03/01 1317	300	570	370	200	22	
7		03/03 1900	03/04 2000					03/04 0810	130	580	390	190	12.2	Neugebauer *et al.* (2004) has different view, entropy hole
8	5	03/28 1200	03/30 1948					03/29 0617	150	560	320	240	15.5	
9	6	04/10 0230	04/10 2230					04/10 0630	115	600	350	250	13	A trough of P_t
10		04/20 1300	04/20 2310					04/20 1635	130	660	470	190	13	ACE
11	7	04/28 1000	04/30 1100					04/29 1500	85	650	400	250	10	
12		05/12 2200	05/13 2000					05/13 0602	190	515	380	135	19	Big disturbance of V_P before the event
13	8	05/18 0032	05/18 1948	05/18 0032	F	38 → 163	125	05/18 0549	360	700	340	360	28	Classic

(*Continued on next page*)

(*Continued*)

SIR #	CIR #	Start UT [mm/dd hhmm]	End UT [mm/dd hhmm]	Discontinuity UT [mm/dd hhmm]	F/R[a] Shock	ΔP^b (pPa)		Stream interface (SI) UT [mm/dd hhmm]	P_{max} (pPa)	V_{max} (km s^{-1})	V_{min} (km s^{-1})	ΔV^c (km s^{-1})	B_{max} (nT)	Comments
				05/18 1948	R	80 → 20	−60							
14		05/23 0030	05/23 1930					05/23 0847	75	512	380	132	9.6	A trough of P_t
15	9	05/24 0900	05/25 1030	05/25 1008	R	70 → 20	−50	05/25 0426	240	605	400	205	15	
16	10	06/08 0000	06/09 0530					06/08 0746	132	660	340	320	12.2	
17		06/15 0600	06/18 0000					06/15 1211	87	410	280	130	11	P_t plateau, a small trough of P_t in the center
18*	11	06/26 0200	06/28 1000	06/26 0232	F	65 → 150	85	06/26 1937	460	910	307	603	25	ICME + SIR
				06/26 1932	F	120 → 395	275							
19		07/14 1200	07/15 2230					07/15 0000	80	426	300	126	9.7	A small trough of P_t
20	12	07/21 1300	07/22 2200					07/22 0900	220	540	275	265	19.6	
21*	13	07/30 0600	07/31 0000					07/30 1912	285	670	380	290	24	ACE, followed by several ICMEs
22		08/06 0500	08/06 2200					08/06 1020	112	500	322	178	12.4	
23*		08/09 2130	08/12 0200					08/11 0156	132	435	300	135	14.5	Following an ICME
24	14	08/15 1033	08/17 0216	08/15 1033	F	50 → 123	73	08/15 2054	270	680	340	340	21.6	
				08/17 0216	R	80 → 35	−45							

(*Continued on next page*)

(*Continued*)

SIR #	CIR #	Start UT [mm/dd hhmm]	End UT [mm/dd hhmm]	Discontinuity UT [mm/dd hhmm]	F/R[a] Shock	ΔP^{b} (pPa)		Stream interface (SI) UT [mm/dd hhmm]	P_{max} (pPa)	V_{max} (km s^{-1})	V_{min} (km s^{-1})	ΔV^{c} (km s^{-1})	B_{max} (nT)	Comments
25*	15	08/23 0600	08/24 2000	08/23 1211	F	40 → 81	41	08/23 1721	150	538	380	158	16	P_t increases in steps, closely following an ICME
				08/23 1542	F	75 → 115	40							
26		09/07 0100	09/08 0000					09/07 0750	157	535	353	182	14.5	Neugebauer *et al.* (2004)
27	16	09/12 0358	09/13 1900	09/12 0358	F	36 → 87	51	09/12 1613	185	662	410	252	15	V_P and P_t irregular
28	17	09/26 0800	09/27 1800	09/26 1456	F	100 → 157	57	09/26 1934	280	690	340	350	18	
				09/26 1851	/	167 → 232	65							
				09/26 2015	/	205 → 135	−70							
29	18	10/09 1600	10/11 0700					10/10 1336	300	685	380	305	17.5	
30*	19	10/21 0221	10/22 1300	10/21 0221	F	73 → 383	310	10/22 0638	610	720	347	373	38	ICME + SIR, a trough of P_t in the center
31		10/31 0000	11/01 0900	11/01 0609	R	85 → 45	−40	10/31 1010	135	473	360	113	14.3	ACE, weak
32	20	11/05 2003	11/09 0000	11/05 2003	F	38 → 67	29	11/07 1415	270	663	315	348	18	V_P irregular
				11/08 0134	/	110 → 46	−64							
33*		11/21 1400	11/24 0640	11/21 1713	/	85 → 126	41	11/22 0156	200	510	350	160	16.3	T_P and V_P irregular, SIR + ICME

(*Continued on next page*)

(*Continued*)

SIR #	CIR #	Start UT [mm/dd hhmm]	End UT [mm/dd hhmm]	Discontinuity UT [mm/dd hhmm]	F/R[a] Shock	ΔP^b (pPa)		Stream interface (SI) UT [mm/dd hhmm]	P_{max} (pPa)	V_{max} (km s^{-1})	V_{min} (km s^{-1})	ΔV^c (km s^{-1})	B_{max} (nT)	Comments
34	21	12/02 0600	12/05 0000					12/04 0506	240	750	330	420	21	ACE
35	22	12/23 1142	12/25 0600					12/24 0644	330	647	264	383	33	*Wind*, |**B**| abnormally high at some points, two peaks, close to Earth; data gap of ACE
36	23	12/30 1030	12/31 1900					12/31 0016	240	720	370	350	19	ACE, classic, *Wind* close to Earth
2000														
1	1	01/10 1200	01/12 1000	01/11 1340	F	130 → 260	130	01/11 1400	310	600	320	280	22.3	ACE, SI in the center, *Wind* was in the magnetosheath
2	2	01/27 0500	01/28 0900	01/27 1357	F	200 → 480	280	01/27 1820	650	750	320	430	31	ACE, high N_P, *Wind* data gap
3	3	02/05 1527	02/07 0000	02/05 1527	F	27 → 55	28	02/05 2114	320	700	372	328	19.7	Classic
4	4	02/23 0400	02/24 1415	02/24 1416	R	230 → 35	−195	02/24 0936	285	760	350	410	17.5	After an ICME
5		03/05 1300	03/07 0600					03/06 0655	86	470	310	160	11.3	Weak, after an ICME

(*Continued on next page*)

(*Continued*)

SIR #	CIR #	Start UT [mm/dd hhmm]	End UT [mm/dd hhmm]	Discontinuity UT [mm/dd hhmm]	F/R[a] Shock	ΔP^{b} (pPa)		Stream interface (SI) UT [mm/dd hhmm]	P_{max} (pPa)	V_{max} ($km\,s^{-1}$)	V_{min} ($km\,s^{-1}$)	ΔV^{c} ($km\,s^{-1}$)	B_{max} (nT)	Comments
6		03/11 2300	03/12 2300					03/12 1130	170	462	310	152	16.2	V_P does not monotonically increase
7		03/16 1052	03/18 0000					03/17 1120	105	338	272	66	12.3	V_P is noisy and does not monotonically increase
8	5	03/22 0100	03/22 1900					03/22 1606	330	595	340	255	23	Noisy
9		03/23 2200	03/24 1930					03/24 0545	54	790	490	300	9.2	Noisy and plateau
10		03/31 1800	04/02 1300					04/01 1615	100	495	355	140	13	
11	6	04/15 1400	04/17 1015	04/14 1935	/	34 → 50	16	04/16 2005	240	530	270	260	17.8	
				04/16 1030	/	110 → 80	−30							
				04/17 1015	R	57 → 25	−32							
12*		04/18 1600	04/20 0200					04/19 1610	90	560	395	165	12.3	ACE, ICME with SIR
13*	7	05/01 1345	05/02 2200	05/01 1345	/	40 → 65	25	05/02 1047	113	900	420	480	16	Big deflection of V_P, containing a tiny flux rope

(*Continued on next page*)

(*Continued*)

SIR #	CIR #	Start UT [mm/dd hhmm]	End UT [mm/dd hhmm]	Discontinuity UT [mm/dd hhmm]	F/R[a] Shock	ΔP^{b} (pPa)	Stream interface (SI) UT [mm/dd hhmm]	P_{max} (pPa)	V_{max} (km s^{-1})	V_{min} (km s^{-1})	ΔV^{c} (km s^{-1})	B_{max} (nT)	Comments
				05/02 1047	/	113 → 90 −23							
14	8	05/12 1500	05/13 2300				05/13 0342	186	610	300	310	17.3	CR[f] think it is followed by an ICME
15		05/17 2000	05/18 1200				05/18 0000	106	640	470	170	13.2	Noisy
16*	9	05/23 1400	05/24 1400				05/24 0140	800	700	520	180	36	ACE, very strong, with ICME
17	10	05/29 0700	05/30 0300				05/29 1617	260	720	330	390	19	30-min data gap
18	11	06/14 0800	06/15 1700				06/14 2000	200	700	410	290	14.5	Classic
19		07/03 1000	07/05 0000				07/04 1247	96	595	320	275	11.7	
20		07/31 1500	08/02 0200				07/31 2113	105	535	363	172	13	
21		08/23 2200	08/25 0600				08/24 0851	135	440	300	140	15.5	A peak before the event
22	12	08/27 1400	08/29 0500				08/28 1610	130	650	332	318	12	Irregular P_t
23		09/11 1000	09/13 1200				09/12 1831	100	455	330	125	11.3	
24	13	09/16 1830	09/17 1100				09/16 2310	175	588	350	238	17	Followed by an ICME
25	14	09/24 1200	09/25 0400				09/24 2202	110	580	380	200	13.2	

(*Continued on next page*)

(*Continued*)

SIR #	CIR #	Start UT [mm/dd hhmm]	End UT [mm/dd hhmm]	Discontinuity UT [mm/dd hhmm]	F/R[a] Shock	ΔP^{b} (pPa)		Stream interface (SI) UT [mm/dd hhmm]	P_{max} (pPa)	V_{max} ($km\,s^{-1}$)	V_{min} ($km\,s^{-1}$)	ΔV^{c} ($km\,s^{-1}$)	B_{max} (nT)	Comments
26		09/25 0600	09/26 0400					09/25 1354	83	626	460	166	10.8	Closely following an SIR
27	15	10/15 1800	10/16 1200					10/16 0000	85	622	462	160	10.5	Weak, after an ICME
28	16	10/22 0500	10/23 0800					10/22 2320	125	595	355	240	15.6	A trough of P_t
29	17	11/03 2000	11/05 1800	11/04 0225	F	75 → 235	160	11/04 0345	320	710	320	390	23.7	A trough of P_t
30		11/23 2200	11/25 0000					11/24 1600	140	550	300	250	14.3	
31	18	12/06 1500	12/09 0400					12/08 0835	160	680	340	340	15	Noisy, BDE[g]
32*		12/24 0800	12/26 1200	12/24 0825	/	44 → 57	13	12/25 0230	170	500	295	205	16.5	BDE
2001														
1		01/02 1305	01/05 0400	01/02 1305	F	35 → 53	18	01/04 1440	130	440	270	170	14	Toughs of T_P and P_t
				01/04 0114	F	40 → 65	25							
2		01/10 1609	01/11 1000	01/10 1609	F	27 → 58	31	01/10 2052	105	490	330	160	12.2	
3	1	01/21 0600	01/22 1800					01/21 2200	240	540	310	230	19.5	
4		01/28 1030	01/29 2000					01/29 0135	200	488	300	188	16.7	Little heating of plasma
5	2	02/05 2000	02/07 1000					02/06 0625	225	540	315	225	16	T_P irregular
6		02/12 2100	02/14 0000	02/12 2131	/	27 → 50	23	02/13 0532	160	630	420	210	15	V_P and P_t irregular
				02/13 0428	/	70 → 140	70							

(*Continued on next page*)

(*Continued*)

SIR #	CIR #	Start UT [mm/dd hhmm]	End UT [mm/dd hhmm]	Discontinuity UT [mm/dd hhmm]	F/R[a] Shock	ΔP[b] (pPa)		Stream interface (SI) UT [mm/dd hhmm]	P_{max} (pPa)	V_{max} (km s^{-1})	V_{min} (km s^{-1})	ΔV[c] (km s^{-1})	B_{max} (nT)	Comments
7		02/26 0400	02/27 1800	02/27 1222	/	170 → 30	−140	02/27 0552	200	400	260	140	14	Noisy, 16-hr data gap of ACE
8	3	02/28 0400	02/28 1600					02/28 0732	125	550	330	220	13.2	Noisy
9*		03/03 0900	03/06 0000	03/03 1040	F	17 → 60	43	03/05 1355	130	600	440	160	14.5	ACE, containing an ICME without BDEs (03/04 0400 – 03/05 0140), a trough of P_t
				03/05 2135	R	53 → 22	−31							
10		05/08 0600	05/09 2025	05/08 1109	F	37 → 87	50	05/08 1116	90	580	350	230	12.3	Noisy deflections of V_P
11	4	05/12 0400	05/12 2200	05/12 1003	F	83 → 128	45	05/12 1235	200	660	380	280	19	N_P compression is not obvious
12		05/13 1100	05/14 0500					05/13 2220	100	625	480	145	13	Close to the previous SIR, noisy, no big deflection of V_P
13*	5	05/22 0000	05/25 2000	05/23 0422	SR[g]			05/23 0250	178	640	295	345	17	Containing an ICME-like structure in the leading part

(*Continued on next page*)

(*Continued*)

SIR #	CIR #	Start UT [mm/dd hhmm]	End UT [mm/dd hhmm]	Discontinuity UT [mm/dd hhmm]	F/R[a] Shock	ΔP^b (pPa)	Stream interface (SI) UT [mm/dd hhmm]	P_{max} (pPa)	V_{max} (km s^{-1})	V_{min} (km s^{-1})	ΔV^c (km s^{-1})	B_{max} (nT)	Comments
14	6	06/01 0700	06/02 1400	06/02 1240	/	115 → 50 −65	06/01 2130	242	570	306	264	22	
15	7	06/08 1200	06/10 0400				06/09 0410	110	640	360	280	12.5	A trough of P_t
16*	8	06/18 0000	06/20 0500				06/18 1310	200	750	300	450	17	P_t irregular, containing a 13-hr ICME-like structure
17		07/13 2100	07/14 0700				07/14 0135	135	450	383	67	14	Followed by another V_P increase, obvious V_P deflection
18	9	07/16 0500	07/17 0900				07/16 1520	120	625	390	235	14	No sharp SI, V_P, N_P, and T_P all gradually change
19	10	07/24 0000	07/26 0000				07/25 0000	90	600	360	240	11	Noisy, no big V_P deflection
20	11	07/30 1600	07/31 2300				07/31 0400	250	625	320	305	19.5	
21		08/09 1800	08/10 1400				08/10 0210	90	480	343	137	10	
22	12	08/21 0000	08/22 1200				08/21 2245	75	660	390	270	11	No big deflection, P_t plateau

(*Continued on next page*)

(*Continued*)

SIR #	CIR #	Start UT [mm/dd hhmm]	End UT [mm/dd hhmm]	Discontinuity UT [mm/dd hhmm]	F/R[a] Shock	ΔP[b] (pPa)		Stream interface (SI) UT [mm/dd hhmm]	P_{max} (pPa)	V_{max} (km s^{-1})	V_{min} (km s^{-1})	ΔV[c] (km s^{-1})	B_{max} (nT)	Comments
23		08/25 0600	08/27 0100					08/25 2100	110	460	342	118	12.6	Troughs of T_P and V_P
24	13	09/02 1600	09/04 0400					09/03 1140	90	560	320	240	10.5	ACE, *Wind* data gap 09/09 1200 – 09/11 1200
25*	14	09/14 1800	09/15 1900	09/14 2059	SR[g]	65 → 60	−5	09/15 0505	100	610	400	210	11.5	ACE, ICME with SIR
26	15	09/23 0300	09/24 0700					09/23 0919	230	585	340	245	18.5	
27		10/08 0400	10/09 1600	10/08 1305	F	70 → 112	42	10/08 1445	140	485	340	145	14.6	No big deflection, several data gaps during 11/01 – 11/16, some data gaps at SIRs in Nov. and Dec.
28*	16	10/11 1620	10/12 0900	10/11 1620	F	80 → 340	260	10/11 2210	480	600	360	240	28	ACE, SIR + ICME, short interval for ICME, ∼6 hours, BDE for over three days

(*Continued on next page*)

(*Continued*)

SIR #	CIR #	Start UT [mm/dd hhmm]	End UT [mm/dd hhmm]	Discontinuity UT [mm/dd hhmm]	F/R[a] Shock	ΔP^{b} (pPa)		Stream interface (SI) UT [mm/dd hhmm]	P_{max} (pPa)	V_{max} (km s^{-1})	V_{min} (km s^{-1})	ΔV^{c} (km s^{-1})	B_{max} (nT)	Comments
29		12/02 0800	12/04 1800					12/03 2147	180	550	330	220	18.5	ACE, although it is associated with BDEs
30	17	12/14 2100	12/16 1212	12/16 1212	R	86 → 40	−46	12/15 1647	420	570	280	290	26	Irregular and noisy P_t
31		12/21 1000	12/22 0600	12/21 1410	F	58 → 78	20	12/21 1446	100	480	325	155	12.5	
32	18	12/23 2330	12/24 1300	12/23 2330	F	47 → 90	43	12/24 0630	210	590	320	270	18.8	BDEs near the forward shock, a low-latitude coronal hole close to disk center on 12/21
2002														
1		01/07 0900	01/09 0100					01/08 0825	115	475	320	155	13	P_t plateau and noisy
2	1	01/10 1100	01/11 0500	01/10 1627	/	120 → 320	200	01/10 1706	400	673	390	283	22	
3		01/19 0500	01/21 1800					01/19 0907	223	523	288	235	19	A trough of P_t
4		01/24 2100	01/27 0000					01/25 1427	95	500	315	185	12.2	
5	2	02/04 1800	02/06 0600	02/06 0448	R	113 → 53	−60	02/05 2303	420	715	308	407	22	
6		02/10 2000	02/12 1300					02/11 0210	60	600	410	190	9.8	ACE

(*Continued on next page*)

(*Continued*)

SIR #	CIR #	Start UT [mm/dd hhmm]	End UT [mm/dd hhmm]	Discontinuity UT [mm/dd hhmm]	F/R[a] Shock	ΔP^{b} (pPa)		Stream interface (SI) UT [mm/dd hhmm]	P_{max} (pPa)	V_{max} (km s^{-1})	V_{min} (km s^{-1})	ΔV^{c} (km s^{-1})	B_{max} (nT)	Comments
7		02/16 1100	02/17 2000	02/16 1140	/	34 → 43	9	02/17 0431	200	450	308	142	15.2	
				02/17 0332	F	55 → 200	145							
8	3	03/03 1900	03/05 0800	03/03 2338	SR[h]			03/04 1730	320	750	340	410	22.8	Following an ICME
9		03/11 1000	03/12 1500					03/11 1831	140	520	335	185	14.5	Noisy
10	4	03/29 2000	03/31 1600	03/29 2215	F	80 → 190	110	03/30 0023	350	800	314	486	23.5	Two steps of V_P enhancement
				03/31 1551	/	90 → 35	−55							Not a reverse shock due to noisy V_P
11		04/06 2100	04/07 1900					04/07 0620	70	445	320	125	9.7	Entropy hole before the SI
12*		04/10 0000	04/12 1200					04/11 0102	140	550	283	267	14.3	SIR with ICME (04/12 – 04/13 1530)
13		04/27 0800	04/28 0700					04/27 1850	90	540	390	150	11.8	ACE, V_P noisy deflections
14		05/05 1800	05/08 0200					05/07 1100	78	415	310	105	10.2	Two peaks of P_t

(*Continued on next page*)

(*Continued*)

SIR #	CIR #	Start UT [mm/dd hhmm]	End UT [mm/dd hhmm]	Discontinuity UT [mm/dd hhmm]	F/R[a] Shock	ΔP^b (pPa)		Stream interface (SI) UT [mm/dd hhmm]	P_{max} (pPa)	V_{max} (km s^{-1})	V_{min} (km s^{-1})	ΔV^c (km s^{-1})	B_{max} (nT)	Comments
15*		05/11 1000	05/12 1400	05/11 1030	F	60 → 270	210	05/11 1122	320	550	400	150	23	ICME (05/11 1618 – 05/12 0100, T_P not low) + SIR
				05/12 0234	/	48 → 24	−24							
16	5	05/26 1900	05/28 0200					05/27 1232	130	890	400	490	14	
17		06/01 1300	06/03 1800					06/02 2014	95	500	320	180	11.7	
18	6	06/08 0030	06/09 0000	06/08 1028	F	80 → 140	60	06/08 1128	170	440	290	150	15.5	
19		06/15 1600	06/17 0600					06/16 0533	125	428	323	105	12.5	
20	7	06/18 1000	06/19 1800					06/19 0322	210	620	350	270	16.7	
21	8	07/05 0200	07/06 1130					07/06 0858	210	563	333	230	14	P_t plateau
22	9	07/11 2300	07/12 1900					07/12 1107	235	590	380	210	16.6	A small trough of P_t
23		07/15 1900	07/16 1700					07/16 0828	112	435	330	105	10.3	
24		08/11 0245	08/11 2200					08/11 1015	85	540	390	150	9.6	ACE, apparent deflection of V_P
25	10	08/14 0800	08/17 0000					08/15 1900	90	730	420	310	11.2	ACE, very noisy *Wind* data, sharp changes at SI
26		09/03 0200	09/04 1900	09/04 1842	/	56 → 25	−31	09/04 0720	230	495	330	165	19.2	Noisy

(*Continued on next page*)

(*Continued*)

SIR #	CIR #	Start UT [mm/dd hhmm]	End UT [mm/dd hhmm]	Discontinuity UT [mm/dd hhmm]	F/R[a] Shock	ΔP^b (pPa)		Stream interface (SI) UT [mm/dd hhmm]	P_{max} (pPa)	V_{max} ($km\,s^{-1}$)	V_{min} ($km\,s^{-1}$)	ΔV^c ($km\,s^{-1}$)	B_{max} (nT)	Comments
27	11	09/11 0500	09/12 0500					09/11 1507	180	552	390	162	15	V_P noisy
28	12	09/16 0500	09/16 2300					09/16 1434	120	520	340	180	14.5	
29*		09/30 0700	10/02 1200	09/30 0755	F	140 → 360	220	09/30 2100	340	535	290	245	26.5	ICME in SIR
30	13	10/07 0000	10/08 0600					10/07 1250	130	538	340	198	14.8	
31		10/14 0200	10/15 0300					10/14 1439	213	440	260	180	20	SIR + SIR
32	14	10/15 0300	10/16 0400					10/15 1918	310	600	405	195	19	Noisy, following an SIR
33	15	10/23 2000	10/25 0000					10/24 1212	220	790	420	370	18	
34		11/01 0600	11/03 1200					11/02 1342	130	500	400	100	12.5	From ACE, *Wind* data gap
35	16	11/09 1600	11/11 1800	11/09 1725	F	25 → 50	25	11/11 1227	340	710	340	370	19.8	
				11/09 1827	F	48 → 135	87							
				11/13 0457	R	90 → 50	−40							
36*	17	11/20 1000	11/21 1300	11/20 1050	F	63 → 225	162	11/21 0200	850	785	350	435	41	Seem to contain a flux rope
37	18	12/06 1100	12/07 1900					12/07 0908	310	630	370	260	18	
38	19	12/13 1900	12/15 1500					12/14 2110	180	615	342	273	15	
39*		12/17 2230	12/19 2100	12/19 1852	R	75 → 43	−32	12/19 0519	300	540	340	200	23	ACE, ICME + SIR
40		12/22 0700	12/23 1030	12/22 1217	/	120 → 200	80	12/22 2127	220	600	370	230	21.5	ACE, irregular P_t
41	20	12/26 1400	12/27 1500					12/26 2323	250	760	383	377	16.8	

(*Continued on next page*)

(*Continued*)

SIR #	CIR #	Start UT [mm/dd hhmm]	End UT [mm/dd hhmm]	Discontinuity UT [mm/dd hhmm]	F/R[a] Shock	ΔP^b (pPa)		Stream interface (SI) UT [mm/dd hhmm]	P_{max} (pPa)	V_{max} (km s^{-1})	V_{min} (km s^{-1})	ΔV^c (km s^{-1})	B_{max} (nT)	Comments
2003														
1	1	01/02 1600	01/04 0700					01/03 1715	150	660	360	300	15.3	A trough of P_t
2		01/09 1200	01/11 1200					01/10 0720	125	500	270	230	14	6-hr data gap
3	2	01/17 0000	01/20 0000					01/18 2226	180	640	320	320	17	No sharp SI
4	3	02/03 0600	02/05 0000					02/04 0537	115	710	460	250	12.6	Noisy
5	4	02/12 1600	02/15 1600					02/14 0842	140	675	360	315	15.5	ACE, three peaks of P_t
6		02/19 1200	02/20 1500					02/20 0410	100	730	510	220	11	T_P irregular, troughs of T_P and P_t
7	5	02/26 1700	02/27 1335	02/26 2225	/	210 → 165	−45	02/26 2205	210	605	400	205	18	Noisy
				02/27 1335	R	120 → 40	−80							
8		03/03 0400	03/04 1400					03/03 1930	170	610	370	240	16	
9		03/11 1100	03/11 2100					03/11 1530	95	500	380	120	12	Sharp SI
10	6	03/13 1800	03/15 0000					03/14 0518	130	650	460	190	15	N_P and T_P jump at different places
11		03/26 1400	03/28 0000	03/26 1640	/	31 → 54	23	03/27 0032	130	550	370	180	12	No V_P big deflection
				03/27 0032	/	130 → 100	−30							
12	7	03/29 1800	03/31 0000					03/30 0049	150	650	380	270	14	Two stages of V_P increase

(*Continued on next page*)

(*Continued*)

SIR #	CIR #	Start UT [mm/dd hhmm]	End UT [mm/dd hhmm]	Discontinuity UT [mm/dd hhmm]	F/R[a] Shock	ΔP^{b} (pPa)		Stream interface (SI) UT [mm/dd hhmm]	P_{max} (pPa)	V_{max} ($km\,s^{-1}$)	V_{min} ($km\,s^{-1}$)	ΔV^{c} ($km\,s^{-1}$)	B_{max} (nT)	Comments
13	8	04/07 0600	04/11 0200	04/08 0020	F	60 → 160	100	04/08 0855	250	750	370	380	18	A trough of P_t
14	9	04/13 1800	04/16 1800					04/14 1600	110	790	440	350	14	A trough of P_t
15		04/24 0800	04/25 0100					04/24 1335	90	610	430	180	11.5	Noisy
16	10	05/04 1900	05/06 1200	05/04 1911	/	46 → 56	10	05/05 1840	210	750	360	390	17	
17		05/21 0700	05/22 0800					05/21 1915	120	580	400	180	14.5	Irregular T_P
18		05/27 0000	05/28 1500					05/27 2100	110	770	450	320	12.5	
19	11	06/01 0000	06/03 0600					06/01 2326	125	900	580	320	12	Quite noisy
20		06/14 0800	06/15 0400	06/14 2240	/	130 → 65	−65	06/14 2115	200	600	450	150	18	Irregular V_P
21*		06/18 0442	06/19 0400	06/18 0442	F	70 → 143	73	06/18 1018	180	650	450	200	19	After an ICME, one stream quiet, the other one noisy
22	12	06/26 0600	06/27 1300					06/26 1335	175	750	500	250	17	
23		07/03 0900	07/04 1200					07/03 2208	130	820	460	360	12	
24*	13	07/11 0000	07/12 2000	07/12 0847	/	80 → 25	−55	07/11 1632	170	680	340	340	17	
25	14	07/26 0600	07/27 0700	07/26 1940	/	550 → 670	120	07/26 2155	650	800	340	460	35	
				07/27 0512	/	175 → 25	−150							
26		07/28 0600	07/29 0800					07/28 1255	100	820	550	270	12	Closely following a CIR
27*		08/05 1800	08/06 1600					08/06 0046	120	550	410	140	13.5	Closely following an ICME

(*Continued on next page*)

(*Continued*)

SIR #	CIR #	Start UT [mm/dd hhmm]	End UT [mm/dd hhmm]	Discontinuity UT [mm/dd hhmm]	F/R[a] Shock	ΔP^{b} (pPa)	Stream interface (SI) UT [mm/dd hhmm]	P_{max} (pPa)	V_{max} (km s^{-1})	V_{min} (km s^{-1})	ΔV^{c} (km s^{-1})	B_{max} (nT)	Comments
28	15	08/07 0800	08/08 1000				08/08 0425	130	800	460	340	14	Noisy, two stages of V_P increase
29	16	08/20 1000	08/22 0700				08/21 0840	170	770	435	335	16.2	ACE, P_t zigzag
30		08/29 0700	08/30 0200				08/29 2030	100	640	430	210	12.5	
31		08/31 2200	09/02 1200				09/01 0441	115	570	392	178	13.7	ACE, two stages of V_P increase
32	17	09/03 1400	09/04 2300				09/04 0800	75	700	470	230	11.2	ACE, no obvious SI
33	18	09/08 1300	09/10 0400				09/09 1855	250	670	375	295	16	Irregular P_t
34	19	09/15 1900	09/17 1900	09/15 1945	/	30 → 70 40	09/16 2017	280	780	350	430	23	Classic, but no sharp T_P increase
35	20	10/01 1200	10/03 1800				10/01 2300	150	500	280	220	18.5	V_P and T_P increase irregularly, V_P deflects greatly
36		10/05 1230	10/06 0900				10/05 2312	140	470	360	110	14.2	Closely followed by another SIR
37	21	10/06 0900	10/07 0100				10/06 2030	140	650	380	270	14	Irregular increases of V_P and T_P

(*Continued on next page*)

(*Continued*)

SIR #	CIR #	Start UT [mm/dd hhmm]	End UT [mm/dd hhmm]	Discontinuity UT [mm/dd hhmm]	F/R[a] Shock	ΔP^b (pPa)	Stream interface (SI) UT [mm/dd hhmm]	P_{max} (pPa)	V_{max} (km s^{-1})	V_{min} (km s^{-1})	ΔV^c (km s^{-1})	B_{max} (nT)	Comments
38	22	10/14 0700	10/15 0900				10/14 1852	285	750	430	320	20	ACE, data gap (10/28 1300 – 10/31 0100)
39		11/08 0400	11/09 1900				11/08 1515	140	600	407	193	14	ACE
40	23	11/10 0900	11/11 2100				11/10 2325	160	780	450	330	16.5	ACE
41		11/29 2230	11/30 1900	11/30 0246	/	70 → 105 35	11/30 0404	190	500	382	118	17	ACE, no sharp SI, parameters gradually change
42		12/04 1800	12/06 0500				12/05 0443	220	560	340	220	18.5	ACE, no sharp T_P increase
43	24	12/07 1000	12/10 1200	12/07 1342	F	40 → 130 90	12/07 1408	150	800	400	400	15	ACE, V_P big deflection
44	25	12/20 0000	12/22 0000				12/20 1225	270	640	308	332	22	ACE, no sharp SI
45		12/26 1800	12/29 0600	12/27 0911	/	48 → 120 72	12/27 0912	115	580	370	210	13.5	ACE, sharp SI
2004													
1	1	01/02 1500	01/03 2000				01/03 0231	140	640	425	215	14.7	ACE, gradual transition between two streams

(*Continued on next page*)

(*Continued*)

SIR #	CIR #	Start UT [mm/dd hhmm]	End UT [mm/dd hhmm]	Discontinuity UT [mm/dd hhmm]	F/R[a] Shock	ΔP[b] (pPa)		Stream interface (SI) UT [mm/dd hhmm]	P_{max} (pPa)	V_{max} (km s^{-1})	V_{min} (km s^{-1})	ΔV[c] (km s^{-1})	B_{max} (nT)	Comments
2		01/06 1926	01/07 1600	01/06 1926	F	30 → 90	60	01/06 2214	160	780	580	200	18	ACE, V_P is noisy
3	2	01/15 0000	01/17 0000					01/15 1445	85	660	420	240	12.7	ACE
4	3	01/29 2025	01/30 1700					01/30 0818	163	700	410	290	17	ACE
5		01/31 0200	01/31 1845					01/31 0730	68	660	420	240	10.2	ACE, weak, P_t plateau, no sharp SI, closely following another SIR
6		02/05 0600	02/06 1200					02/05 2300	54	620	460	160	8.5	ACE, weak
7	4	02/11 0130	02/12 1400					02/12 0230	230	700	350	350	21.3	ACE, classic
8	5	02/26 1930	02/29 2000					02/27 2016	160	750	300	450	17.8	ACE, *Wind* was in magnetosphere
9	6	03/09 1030	03/10 1400	03/10 0741	/	135 → 80	−55	03/09 2050	200	780	400	380	18	
10	7	03/25 0800	03/27 2200					03/25 2150	125	900	350	550	14.8	
11		03/28 1600	03/29 1830					03/29 0617	150	560	320	240	15.5	Excluding an ICME
12*	8	04/05 0800	04/07 0000					04/05 2102	200	633	370	263	19.3	ICME + SIR, nice rope
13	9	04/22 0300	04/25 2000					04/23 1117	120	560	370	280	13.5	

(*Continued on next page*)

(*Continued*)

SIR #	CIR #	Start UT [mm/dd hhmm]	End UT [mm/dd hhmm]	Discontinuity UT [mm/dd hhmm]	F/R[a] Shock	ΔP^{b} (pPa)	Stream interface (SI) UT [mm/dd hhmm]	P_{max} (pPa)	V_{max} ($km\,s^{-1}$)	V_{min} ($km\,s^{-1}$)	ΔV^{c} ($km\,s^{-1}$)	B_{max} (nT)	Comments
14		04/28 0000	04/29 0400				04/28 1630	63	600	410	190	9.8	ACE, no sharp SI
15		05/03 1900	05/04 0700				05/04 0133	75	435	332	103	9	
16	10	05/05 0200	05/06 0400				05/05 1817	130	645	400	245	13	ACE, two stages of V_P enhancement
17	11	05/19 1100	05/22 2300				05/20 1045	140	580	300	280	15.3	Two peaks of P_t
18	12	05/28 0000	05/31 1000				05/30 2245	95	550	420	130	11	A trough of P_t
19*	13	06/13 0000	06/15 2000				06/15 0935	130	560	320	240	13	Containing an ICME-like structure
20	14	06/27 2200	06/29 1000				06/29 0406	200	620	320	300	17.5	
21	15	07/10 0200	07/12 0500	07/12 0455	/	110 → 40 −70	07/12 0125	170	600	285	315	16	No sharp SI, wave has not been compressed into shock at the discontinuity
22		07/16 0300	07/17 1200				07/17 0030	160	575	370	205	18	Disturbances of T_P
23		07/19 0800	07/20 1600				07/19 1515	52	570	360	210	8.8	ACE, weak

(*Continued on next page*)

(*Continued*)

SIR #	CIR #	Start UT [mm/dd hhmm]	End UT [mm/dd hhmm]	Discontinuity UT [mm/dd hhmm]	F/R[a] Shock	ΔP^{b} (pPa)	Stream interface (SI) UT [mm/dd hhmm]	P_{max} (pPa)	V_{max} (km s^{-1})	V_{min} (km s^{-1})	ΔV^{c} (km s^{-1})	B_{max} (nT)	Comments
24		08/06 1400	08/07 2200				08/07 0918	160	475	330	145	15	Followed by another SIR
25	16	08/09 1500	08/10 2100				08/10 0337	110	570	350	220	14	
26		08/25 0400	08/27 1600				08/26 1820	75	475	310	165	10	
27*	17	08/31 0100	09/01 0800				08/31 0735	90	540	390	150	11.5	Closely after an ICME
28		09/04 1800	09/07 0600				09/05 1500	86	470	300	170	13	7-hr data gap
29		09/27 0100	09/29 0700				09/28 0500	75	420	322	98	9.5	No big increase of T_P
30		10/07 2200	10/09 0700				10/08 1722	95	393	280	113	10	Weak
31	18	10/12 2130	10/14 1300				10/13 1236	120	550	380	170	12	T_P irregular
32		10/18 0800	10/21 1600				10/20 1016	110	460	293	167	11.5	
33	19	10/23 2000	10/25 1700				10/25 0451	130	520	340	180	11	No big increase of T_P
34		10/29 0500	10/31 1800				10/29 2127	100	480	297	183	10.3	
35		11/02 1400	11/05 0300				11/03 2332	100	470	332	138	10	T_P irregular

(*Continued on next page*)

(*Continued*)

SIR #	CIR #	Start UT [mm/dd hhmm]	End UT [mm/dd hhmm]	Discontinuity UT [mm/dd hhmm]	F/R[a] Shock	ΔP[b] (pPa)	Stream interface (SI) UT [mm/dd hhmm]	P_{max} (pPa)	V_{max} (km s^{-1})	V_{min} (km s^{-1})	ΔV[c] (km s^{-1})	B_{max} (nT)	Comments
36	20	11/19 1200	11/21 0100	11/21 0042	R	93 → 32 −61	11/19 1730	200	640	340	300	18.2	Two stages of interaction, a trough of P_t
37	21	11/28 1000	11/30 1500				11/29 0057	200	710	360	350	17.8	
38	22	12/15 1400	12/17 2100				12/17 0109	150	680	340	340	11.5	A trough of P_t
39		12/21 0300	12/21 1200				12/21 0720	165	490	350	140	17.2	Closely followed by another SIR
40		12/21 2200	12/22 1800				12/22 0542	165	550	385	165	14.2	
41		12/24 1800	12/27 2200				12/25 1110	120	560	350	210	13.6	

[a]F/R Shock: forward/reverse shock.
[b]ΔP: instantaneous change in total perpendicular pressure (P_t) across the discontinuity, in the unit of pico-Pascal (pPa), "/" means not a shock.
[c]ΔV: change in solar-wind velocity magnitude during one event.
[d]ICME: interplanetary coronal mass ejection.
[e]ACE: from ACE data.
[f]CR: from the list of Cane and Richardson (2003) and private communication in 2006.
[g]BDE: bidirectional solar-wind electron strals.
[h]SR: slow reverse shock, from Kasper's shock list of *Wind* (*http://space.mit.edu/home/jck/shockdb/shockdb.html*).
*Hybrid case consisting of more than one event.

Acknowledgements

This work is supported by the IGPP branch at Los Alamos National Lab (LANL). We have used the *Wind* plasma and magnetic-field data throughout. We thank the MIT and Goddard plasma team (A.J. Lazarus and K.W. Ogilvie), 3DP plasma team (R.P. Lin), and the magnetometer team (R.P. Lepping) for making these data available. We have incorporated ACE data in this study. We are grateful to the PIs of the plasma analyzer (D.J. McComas) and the magnetometer (C.W. Smith) for making these data publicly available, and also thank J.T. Steinberg for collaboration at LANL. Work at Los Alamos was performed under the auspices of the U.S. Department of Energy, with financial support from the NASA ACE program. To identify the shocks, we have used the higher time resolution data in CDAWeb. We thank CDAWeb and the original PIs for making the data available.

References

Bame, S.J., Goldstein, B.E., Gosling, J.T., Harvey, J.W., McComas, D.J., Neugebauer, M., and Phillips, J.L.: 1993, *Geophys. Res. Lett.* **20**(21), 2323, doi: 10.1029/93GL02630.

Belcher, J.W. and Davis, L., Jr.: 1971, *J. Geophys. Res.* **76**, 3534.

Bobrov, M.S.: 1983, *Planet Space Sci.* **31**, 865.

Brueckner, G.E., Howard, R.A., Koomen, M.J., Korendyke, C.M., Michels, D.J., Moses, J.D., Socker, D.G., Dere, K.P., Lamy, P.L., Llebaria, A., Bout, M.V., Schwenn, R., Simnett, G.M., Bedford, D.K., and Eyles, C.J.: 1995, *Solar Phys.* **162**, 357.

Burlaga, L.F.: 1974, *J. Geophys. Res.* **79**, 3717.

Cane, H.V. and Richardson, I.G.: 2003, *J. Geophys. Res.* **108**(A4), 1156, doi: 10.1029/2002JA009817.

Carovillano, R.L. and Siscoe, G.L.: 1969, *Solar Phys.* **8**, 401.

Feldman, W.C., Asbridge, J.R., Bame, S.J., Fenimore, E.E., and Gosling, J.T.: 1981, *J. Geophys. Res.* **86**, 5408.

Formisano, V. and Chao, J.K.: 1972, in K. Schindler (ed.), *Cosmic Plasma Physics*, Plenum, New York, p. 103.

Gosling, J.T.: 1990, in C.T. Russell, E.R. Priest, and L.C. Lee (eds.), *Physics of Magnetic Flux Ropes*, *Geophys. Monogr. Ser.* **58**, AGU, Washington, DC, p. 343.

Gosling, J.T. and Pizzo, V.J.: 1999, *Spa. Sci. Rev*. **89**, 21.

Gosling, J.T., Hundhausen, A.J., and Bame, S.J.: 1976, *J. Geophys. Res.* **81**, 2111.

Gosling, J.T., Hundhausen, A.J., Pizzo, V., and Asbridge, J.R.: 1972, *J. Geophys. Res*. **77**, 5442.

Gosling, J.T., Asbridge, J.R., Bame, S.J., and Feldman, W.C.: 1978, *J. Geophys. Res.* **83**, 1401.

Gosling, J.T., Borrini, G., Asbridge, J.R., Bame, S.J., Feldman, W.C., and Hansen, R.F.: 1981, *J. Geophys. Res.* **86**, 5438.

Gosling, J.T., Baker, D.N., Bame, S.J., Feldman, W.C., Zwickl, R.D., and Smith, E.J.: 1987, *J. Geophys. Res.* **92**, 8519.

Gosling, J.T., Bame, S.J., McComas, D.J., Phillips, J.L., Pizzo, V.J., Goldstein, B.E., and Neugebauer, M.: 1993, *Geophys. Res. Lett*. **20**, 2789.

Gosling, J.T., McComas, D.J., Phillips, J.L., Weiss, L.A., Pizzo, V.J., Goldstein, B.E., and Forsyth, R.J.: 1994, *Geophys. Res. Lett*. **21**, 2271.

Gosling, J.T., McComas, D.J., Skoug, R.M., and Forsyth, R.J.: 2001, *Space Sci. Rev.* **67**, 189.

Hu, Y.Q.: 1993, *J. Geophys. Res.* **98**, 13201.
Hundhausen, A.J.: 1972, *Coronal Expansion and Solar Wind*, Springer-Verlag, New York.
Hundhausen, A.J.: 1973, *J. Geophys. Res.* **78**, 1528.
Hundhausen, A.J.: 1977, in J.B. Zirker (ed.), *Coronal Holes and High Speed Wind Streams*, Colorado Assoc. Univ. Press, Boulder, p. 225.
Hundhausen, A.J. and Gosling, J.T.: 1976, *J. Geophys. Res.* **81**, 1436.
Intriligator, D.S. and Siscoe, G.L.: 1994, *Geophys. Res. Lett.* **21**, 1117.
Issautier, K., Perche, C., Hoang, S., Lacombe, C., Maksimovic, M., Bougeret, J.-L., and Salem, C.: 2005, *Adv. Space Res.* **35**, 2141.
Jian, L., Russell, C.T., Gosling, J.T., and Luhmann, J.G.: 2005a, in B. Fleck, T. H. Zurbuchen, and H. Lacoste (eds.), *Proceedings of Solar Wind 11-SOHO 16, Connecting Sun and Heliosphere*, SP-592 ESA, Noordwijk, The Netherlands, p. 491.
Jian, L., Russell, C.T., Gosling, J.T., and Luhmann, J.G.: 2005b, in B. Fleck, T. H. Zurbuchen, and H. Lacoste (eds.), *Proceedings of Solar Wind 11-SOHO 16, Connecting Sun and Heliosphere*, SP-592 ESA, Noordwijk, The Netherlands, p. 731.
Jian, L., Russell, C.T., Luhmann, J.G., and Skoug, R.: 2006, *Solar Phys.*, doi: 10.1007/s11207-006-0133-2.
Jones, G.H., Balogh, A., and Smith, E.J.: 2003, *Geophys. Res. Lett.* **30**(19), 8028.
Krieger, A.S., Timothy, A.F., and Roelof, E.C.: 1973, *Solar Phys.* **29**, 505.
Lepping, R.P., Acuna, M.H., Burlaga, L.F., Farrell, W.M., Slavin, J.A., Schatten, K.H., Mariani, F., Ness, N.F., Neubauer, F.M., Whang, Y.C., Byrnes, J.B., Kernnon, R.S., Panetta, P.V., Scheifele, J., and Worley, E.M.: 1995, *Space Sci. Rev.* **71**, 207.
Lin, R.P., Anderson, K.A., Ashford, S., Carlson, C., Curtis, D., Ergun, R., Larson, D., McFadden, J., McCarthy, M., Parks, G.K., Reme, H., Bosqued, J.M., Coutelier, J., Cotin, F., D'Uston, C., Wenzel, K.P., Sanderson, T.R., Henrion, J., Ronnet, J.C., and Paschmann, G.: 1995, *Space Sci. Rev.* **71**, 125.
Lindsay, G.M., Russell, C.T., Luhmann, J.G., and Gazis, P.: 1994, *J. Geophys. Res.* **99**, 11.
McComas, D.J., Elliott, H.A., and von Steiger, R.: 2002, *Geophys. Res. Lett.* **29**, 1314.
McComas, D.J., Bame, S.J., Barker, P., Feldman, W.C., Phillips, J.L., Riley, P., and Griffee, J.W.: 1998, *Space Sci. Rev.* **86**, 563.
McComas, D.J., Elliott, H.A., Gosling, J.T., and Skoug, R.M.: 2006, *Geophys. Res. Lett.* **33**, L09102.
Neugebauer, M., Liewer, P.C., Goldstein, B.E., Zhou, X., and Steinberg, J.T.: 2004, *J. Geophys. Res.* **109**, doi: 10.1029/2004JA010456.
Newbury, J.A., Russell, C.T., Phillips, J.L., and Gary, S.P.: 1998, *J. Geophys. Res*. **103**(A5), 9553.
Nolte, J.T., Krieger, A.S., Timothy, A.F., Gold, R.E., Roelof, E.C., Vaiana, G., Lazarus, A.J., Sullivan, J.D., and McIntosh, P.S.: 1976, *Solar Phys.* **46**, 303.
Ogilvie, K.W.: 1972, in P.J. Coleman, C.P. Sonett, and J.M. Wilcox (eds.), *Proceedings of Solar Wind*, NASA SP-308, Washington, DC, p. 430.
Ogilvie, K.W., Chornay, D.J., Fritzenreiter, R.J., Hunsaker, F., Keller, J., Lobell, J., Miller, G., Scudder, J.D., Sittler, E.C.Jr., Torbert, R.B., Bodet, D., Needell, G., Lazarus, A.J., Steinberg, J.T., Tappan, J.H., Mavretic, A., and Gergin, E.: 1995, *Space Sci. Rev.* **71**, 55.
Parker, E.N.: 1963, *Interplanetary Dynamical Processes*, Wiley, New York.
Pizzo, V.J.: 1978, *J. Geophys. Res.* **83**, 5563.
Pizzo, V.J.: 1989, *J. Geophys. Res.* **94**, 8673.
Pneuman, G.W. and Kopp, R.A.: 1971, *Solar Phys*. **18**, 258.
Richter, A.K. and Luttrell, A.H.: 1986, *J. Geophys. Res.* **91**, 5873.
Russell, C.T., Shinde, A.A., and Jian, L.: 2005, *Adv. Space Res.* **35**, 2178.
Sarabhai, V.: 1963, *J. Geophys. Res.* **68**, 1555.
Siscoe, G.L.: 1972, *J. Geophys. Res.* **77**, 27.

Smith, E.J. and Wolfe, J.H.: 1976, *J. Geophys. Res.* **3**, 137.
Smith, C.W., L'Heureux, J., Ness, N.F., Acuña, M.H., Burlaga, L.F., and Scheifele, J.: 1998, *Space Sci. Rev.* **86**, 613.
Wimmer-Schweingruber, R.F., von Steiger, R., and Paerli, R.: 1997, *J. Geophys. Res.* **102**, 17407.
Wimmer-Schweingruber, R.F., von Steiger, R., and Paerli, R.: 1999, *J. Geophys. Res.* **104**, 9933.